HHS Public Access

Author manuscript

Nat Cell Biol. Author manuscript; available in PMC 2021 January 15.

Published in final edited form as:

Nat Cell Biol. 2020 March ; 22(3): 266–273. doi:10.1038/s41556-020-0465-4.

A negative feedback loop maintains optimal chemokine concentrations for directional cell migration

Stephanie Lau[1], **Anna Feitzinger**[1], **Gayatri Venkiteswaran**[1], **John Wang**[1], **Stephen W. Lewellis**[1], **Chad A. Koplinski**[2], **Francis C. Peterson**[2], **Brian F. Volkman**[2], **Martin Meier-Schellersheim**[3,*], **Holger Knaut**[1,*]

[1]Skirball Institute of Biomolecular Medicine, New York University School of Medicine, 540 First Avenue, New York, NY 10016, USA

[2]Department of Biochemistry, Medical College of Wisconsin, Milwaukee, WI 53226, USA

[3]Laboratory of Systems Biology, National Institute of Allergy and Infectious Diseases, National Institutes of Health, Bethesda, Maryland, USA.

Abstract

Chemoattractant gradients often guide migrating cells. To achieve the greatest directional signal over noise, such gradients should be maintained with concentrations around the chemoreceptor's dissociation constant (K_d) [1–6]. Whether this is true in animals is unknown. Here, we investigate whether a moving tissue, the zebrafish posterior lateral line primordium, buffers its attractant in this concentration range for robust migration. We find that the Cxcl12/Sdf1 attractant gradient ranges from 0 to 12 nM and thus borders around the 3.4 nM K_d of its receptor Cxcr4. When we increase the Cxcl12-Cxcr4 K_d, primordium migration is less directional. Furthermore, a negative feedback loop between Cxcl12 and its clearance receptor Ackr3/Cxcr7 regulates the Cxcl12 concentrations. Breaking this negative feedback by blocking the phosphorylation of Ackr3b's cytoplasmic tail also results in less directional primordium migration. Thus, the primordium relies on a close match between the Cxcl12 concentration and the Cxcl12-Cxcr4 K_d for directed migration which it maintains by buffering the chemokine levels. Quantitative modeling confirms the plausibility of this mechanism. We anticipate that attractant concentration buffering is a general mechanism to ensure robust cell migration.

Theoretical considerations and cell culture experiments suggest that the concentration of attractants should be close to the dissociation constant (K_d) of the attractant for its receptor. At these concentrations, small changes in attractant concentration lead to maximal changes

*Correspondence: mms@niaid.nih.gov and holger.knaut@med.nyu.edu.

Author contributions

S.L., M.M-S. and H.K. conceived the project. S.L. and H.K. designed the experiments and analysed the data. S.L. performed the experimental work with the following exceptions: J.W. and A.F. performed experiments involving the quantification of the Cxcl12a concentrations. S.W.L. and G.V. generated and characterized the Ackr3b-GFP expression in zebrafish. C.A.K., F.C.P. and B.F.V. purified the chemokine proteins. M.M-S. performed the computational modeling. H.K. helped with the generation of the transgenic lines. S.L., M.M-S. and H.K. wrote, reviewed and edited the manuscript.

Competing interests

The authors declare no competing interests except B.F.V., C.A.K., and F.C.P. who have ownership interests in Protein Foundry, LLC.

in the attractant-receptor complex concentration and thus a maximal signal to noise ratio [1–6]. Yet the concentration of attractants available for signaling in animals is unknown and whether mechanisms exist that maintain attractant concentrations around receptor K_ds is unclear. To address these questions, we used the zebrafish posterior lateral line primordium (primordium) as a model. The primordium is a collectively migrating tissue that expresses the G-protein coupled chemokine receptor Cxcr4b and migrates over a stripe of Cxcl12a-secreting cells which marks the migratory route [7]. In its back, the primordium expresses the Cxcl12a-clearance receptor Ackr3b which removes the chemokine to generate a local Cxcl12a gradient across the primordium [8,9]. This self-generated gradient directs the primordium forward.

To determine the available Cxcl12a concentrations for signaling (signaling-available Cxcl12a) across the migrating primordium, we used a Cxcl12a-signaling sensor that we previously developed [9]. This sensor consists of Cxcr4b fused to Kate2, an RFP, followed by an IRES that expresses membrane-tethered GFP (Fig. 1a). Binding of Cxcl12a to Cxcr4b-Kate2 induces receptor internalization, resulting in less red fluorescence on the membrane. We previously showed that the ratio of the Kate2 signal to the GFP signal on the membrane is a measure of the fraction of unbound Cxcr4b receptor [9]. Using purified zebrafish Cxcl12a protein (Extended Data Fig. 1a, b) and a cell line that expresses this sensor (Fig. 1b), we calibrated the membrane red-to-green fluorescence intensity ratios and determined the K_d of Cxcl12a for Cxcr4b to be 3.4 nM (Fig. 1d, e, h, Supplementary Table 1). As a validation, we used purified human CXCL12α and a cell line expressing the human CXCL12-signaling sensor and confirmed that this approach reproduces the known K_d of human CXCL12α for human CXCR4 of around 2 nM (Extended Data Fig. 1d, Supplementary Table 1) [10,11]. After correcting for the difference in expression of GFP from the IRES in the Cxcl12a-signaling sensor in cultured cells and embryos (Fig. 1g–h), we used this calibration to calculate the signaling-available Cxcl12a concentrations across the primordium (Fig. 1c, f, g). This analysis showed that the Cxcl12a gradient ranges from 12 nM in the front to close to 0 nM in the back of the primordium (Fig. 1i). The gradient reaches Cxcl12a concentrations around the K_d of its interaction with Cxcr4b at 60 microns from the front of the primordium (Fig. 1i). Thus, much of the primordium is exposed to optimal concentrations of Cxcl12a, which maximizes the signal to noise and is also optimal for shallow gradient sensing.

We then analyzed whether matching the Cxcl12a concentration to its K_d for Cxcr4b is important for the migration of the primordium. Since human and zebrafish ligand-receptor pairs have evolved separately, we reasoned that zebrafish Cxcl12a should bind less tightly to the human CXCR4 receptor than to the zebrafish Cxcr4 receptor. Indeed, the titration of zebrafish Cxcl12a protein on cells expressing the human CXCL12α-signaling sensor showed that the K_d of zebrafish Cxcl12a to human CXCR4 is 782 nM, and thus more than two orders of magnitude higher than the K_d of zebrafish Cxcl12a to zebrafish Cxcr4b (Extended Data Fig. 1e, Supplementary Table 1). Next, we asked whether Cxcl12a also displays a lower affinity, and thus a higher K_d, for the human CXCR4 receptor *in vivo*. A higher K_d should result in less receptor internalization at a given Cxcl12a concentration (Fig. 2a). To test this, we generated transgenic lines that express membrane-tethered Cerulean, a CFP, zebrafish Cxcr4b fused to Citrine, a YFP, and human CXCR4 fused to Kate2 from a genomic fragment on a bacterial artificial chromosome (BAC) that spans the *cxcr4b*

genomic locus (*cxcr4b:Cerulean-CaaX*, *cxcr4b:cxcr4b-Citrine* and *cxcr4b:CXCR4-Kate2*, respectively) (Extended Data Fig. 2a). All the transgenic lines recapitulated the *cxcr4b* expression pattern (Fig. 2b). Using these lines, we measured the membrane fluorescence intensity ratios of zebrafish Cxcr4b-Citrine and human CXCR4-Kate2 to membrane-tethered Cerulean across primordia in *cxcr4b:cxcr4b-Citrine*; *cxcr4b:Cerulean-CaaX* and *cxcr4b:CXCR4-Kate2*; *cxcr4b:Cerulean-CaaX* embryos, respectively. We found that zebrafish Cxcr4b-Citrine was internalized in a graded fashion across the primordium while human CXCR4-Kate2 internalization was only detectable at the front of primordium where Cxcl12a concentrations are highest (Fig. 2b–c). This was also observed when we compared receptor internalization in embryos with increasing Cxcl12a levels over time. Upon over-expression of Cxcl12a from a heat shock promoter, time-lapse imaging showed that the zebrafish Cxcr4b receptor was internalized at lower Cxcl12a levels than the human CXCR4 receptor and with kinetics reflecting the difference in Cxcl12a affinity (Fig. 2d, Extended Data Fig. 2b–d, Video 1). These observations suggest that Cxcl12a has a lower affinity for the human CXCR4 receptor than the zebrafish Cxcr4b receptor *in vitro* and *in vivo*.

To test whether mismatching the ligand concentration and the receptor K_d affects cell migration, we analyzed the behavior of the primordium in *cxcr4b* mutant embryos that instead express zebrafish Cxcr4b-Citrine or human CXCR4-Kate2 from the *cxcr4b* promoter. While zebrafish Cxcr4b-Citrine completely restored primordium migration in *cxcr4b* mutant embryos, human CXCR4-Kate2 migrated slower and in a saltatory manner, completing only 77 % of their migration (Fig. 2e–f and Video 2). Live imaging revealed that the front cells in primordia expressing the human CXCR4 receptor moved at larger angles away from the direction of migration, at more varying speeds, on average more slowly and less directional, and separated further from their neighbors than cells in control primordia expressing the zebrafish Cxcr4b receptor (Extended Data Fig. 2e–h, Video 3–4).

To exclude effects stemming from differences in the signaling behavior between human and zebrafish chemokine receptors, we confirmed these observations by mutating Cxcr4b's binding site for Cxcl12a. Consistent with observations of similar modifications in human CXCR4 [12], replacing two isoleucines with glutamates in the extracellular N-terminal tail of Cxcr4b increased its K_d for Cxcl12a to 21 nM in cells expressing the Cxcl12a-signaling sensor with these changes (Extended Data Fig. 3a–b, Supplementary Table 2). When expressed from the *cxcr4b* regulatory region on a BAC, Cxcr4b^{I7E,I8E}-Kate2 is less internalized than Cxcr4b^{WT}-Kate2 across the primordium (Fig. 3a–c). Similar to primordia guided by the human CXCR4, primordia guided by zebrafish Cxcr4b^{I7E,I8E} also showed migration defects and only completed 66 % of their journey (Fig. 3d–e). These observations suggest that matching the receptor K_d to the ligand concentration is required for robust directional migration and raises the question of how the concentration of signaling-available Cxcl12a is maintained around the K_d of Cxcl12a for Cxcr4b.

Since the alternate Cxcl12a receptor Ackr3b clears Cxcl12a from the extracellular space [13,14], we hypothesized that Ackr3b could respond to changes in Cxcl12a concentration as part of a negative feedback loop (Fig. 4a). To test this idea, we over-expressed Cxcl12a from a heat-shock promoter and measured Ackr3b-GFP (*ackr3b:ackr3b-GFP*) expression from a genomic fragment spanning the *ackr3b* locus on a BAC (Extended Data Fig. 4a). This

transgene recapitulates the endogenous expression pattern of *ackr3b* (Fig. 4b) and rescues the primordium migration defects in *ackr3b* mutant embryos (Extended Data Fig. 4b). In contrast to heat-shocked control embryos, Cxcl12a-over-expressing embryos upregulated Ackr3b-GFP 3.3-fold (Fig. 4b, c, Video 5). We find that by concurrently measuring the internalization of Cxcr4b-GFP from the membrane following Cxcl12a over-expression that Ackr3b-sfGFP upregulation occurs with little lagtime (Extended Data Fig. 4c–d). Thus, Cxcl12a induces the expression of its own clearance receptor Ackr3b rapidly.

One possibility of how Cxcl12a could regulate Ackr3b levels is by increasing *ackr3b* transcription or Ackr3b stability through Cxcr4 signaling. To explore these possibilities, we first over-expressed Cxcl12a in embryos with a transcriptional reporter for *ackr3b*. The *ackr3b* transcriptional reporter drives superfolder GFP (sfGFP) from the *ackr3b* genomic architecture on a BAC (*ackr3b:sfGFP*). This analysis showed that increased Cxcl12a expression did not increase the transcriptional activity of *ackr3b* in heat-shocked control and *hsp70:cxcl12a* embryos (Fig. 4d–f, Video 6). Next, we over-expressed Cxcl12a in *cxcr4a*$^{-/-}$; *cxcr4b*$^{-/-}$ embryos and asked whether this blocks Ack3b-GFP upregulation. In these embryos, Ackr3b-GFP was upregulated to similar levels as in control embryos (Fig. 4g–i, Video 7). These observations suggest that increased *ackr3b* transcription and Cxcr4-mediated Cxcl12a signaling are not the cause for Cxcl12a-induced upregulation of Ackr3b.

Another possibility of how Cxcl12a could regulate Ackr3b levels is by inducing molecular changes that would alter the stability of Ackr3b upon binding (Fig. 5a). The stability of G-protein coupled receptors is often regulated through ubiquitination and phosphorylation of their cytoplasmic tail [15,16]. We therefore generated BAC transgenic lines that express wild-type Ackr3b-sfGFP (Ackr3b$^{\text{wt tail}}$-sfGFP) and, upon Cre-mediated recombination, Ackr3b-sfGFP versions which have lysines or serines and threonines in the cytoplasmic tail mutated to alanines (Ackr3b$^{\text{K/A tail}}$-sfGFP and Ackr3b$^{\text{ST/A tail}}$-sfGFP, Fig. 5b and Extended Data Fig. 5a, b). Importantly, the control *ackr3b: ackr3b*$^{wt\ tail}$*-sfGFP* transgenes restore the migration of the primordium in *ackr3b* mutant embryos (Fig. 5e, Extended Data Fig. 5c). Upon over-expression of Cxcl12a in embryos expressing Ackr3b that cannot be ubiquitinated on its cytoplasmic tail (Ackr3b$^{\text{K/A tail}}$-sfGFP), the mutant clearance receptor was still upregulated (Extended Data Fig. 5a, b, f, g, Video 8). Moreover, the levels of Ackr3b$^{\text{K/A tail}}$-sfGFP were increased 1.4-fold compared to control embryos that express Ackr3b-sfGFP from the same BAC transgene integrated at the same genomic location (Extended Data Fig. 5e). This is consistent with the supposition that ubiquitination dampens Ackr3b receptor levels [17,18]. In contrast to impairing ubiquitination, blocking the phosphorylation of Ackr3b's cytoplasmic tail prevented Cxcl12a-induced Ackr3b$^{\text{ST/A tail}}$-sfGFP upregulation while Ackr3b$^{\text{wt tail}}$-sfGFP levels still increased 4-fold (Fig. 5c–d, Video 9). Expression of Ack3b$^{\text{ST/A tail}}$-sfGFP was also lowered compared to Ackr3b$^{\text{wt tail}}$-sfGFP (Extended Data Fig. 5d). These observations suggest that phosphorylation of the cytoplasmic tail mediates the upregulation of Ackr3b in response to increasing Cxcl12a levels, probably by protecting the receptor from degradation.

To test whether the Cxcl12a-Ackr3b negative feedback loop is essential, we compared the migration of primordia that can upregulate Ackr3b in response to increasing Cxcl12a to primordia that cannot. While embryos expressing Ackr3b$^{\text{wt tail}}$-sfGFP completely rescued

primordia migration of *ackr3b* mutant embryos, embryos expressing Ackr3b$^{ST/A\ tail}$-sfGFP only completed 59 % of their migratory route (Fig. 5e, Extended Data Fig. 5c). Time lapse imaging revealed that primordia in *ackr3b*$^{-/-}$; *ackr3b: ackr3b*$^{ST/A\ tail}$ embryos migrated slower compared to in *ackr3b*$^{-/-}$; *ackr3b: ackr3b*$^{wt\ tail}$ control embryos (Video 10). This suggests that the negative feedback of Ackr3b on Cxcl12a is essential for continued directional migration. Interneuron migration also depends on ACKR3 phosphorylation [17,19], suggesting that the negative feedback of Ackr3b on Cxcl12a levels described here is essential for guidance in other contexts.

Combined, these observations suggest a model in which the dynamic expression of Ackr3b buffers extracellular Cxcl12a concentrations around the K_d of Cxcr4b for Cxcl12a for optimal chemokine attractant sensing. To test this hypothesis quantitatively, we developed a mathematical model that calculates the amount of Cxcl12a-bound Ackr3b receptors that need to be internalized to maintain the measured Cxcl12a gradient. In addition to this gradient, the calculated Ackr3 levels in the model depend on the K_ds of Cxcr4 and Ackr3 for Cxcl12a binding (of which we directly determine the first and computationally deduce the range of the second) and on how much Cxcl12a can be internalized by Cxcr4. The contribution of Cxcr4 is proportional to its experimentally determined expression level on the cells (Fig. 1g, i). The corresponding proportionality factor is the only free parameter in the model. We find that the model can reproduce the experimentally measured Ackr3b distribution across the primordium with high precision (Fig. 5f, Supplementary Note 1, Supplementary Table 3), suggesting that the concentration of Cxcl12a can be buffered by dynamic clearance through Ackr3b (Fig. 5g).

Our study of attractant-guided cell migration in a living animal provides two major insights. First, the signaling-available Cxcl12a concentration in the extracellular space around the migrating primordium closely borders the K_d of Cxcl12a for its receptor Cxcr4b. This is consistent with theoretical considerations and *in vitro* studies indicating that the signal-to-noise is maximal when the attractant concentration matches the attractant receptor's K_d [1,2]. Given that migrating cells frequently have to extract directional information from shallow gradients [20], optimizing the signal-to-noise by matching the attractant concentration to the receptor K_d is probably a general feature in cell migration for robust attractant sensing. Second, we demonstrate that the Cxcl12a concentration is buffered around the K_d for its receptor Cxcr4b through a negative feedback loop with its clearance receptor Ackr3b. This mechanism clamps the attractant's extracellular concentration to ensure the greatest directional signal over noise. Many attractants have negative regulators [21–23] and cells frequently migrate through dynamic and noisy environments during animal development and homeostasis [24,25]. It is therefore likely that other negative regulators feedback on their attractants to optimize the signal-to-noise in directional sensing and buffer the attractant concentration around the attractant receptor K_d for robust cell migration.

Methods

Zebrafish Strains

Zebrafish care and use of live fish for experiments were approved and overseen by the New York University School of Medicine Institutional Animal Care and Use Committee (Protocol

Number: 170105–03). Embryos were raised at 28 degrees C in fish water (0.3g/L Instant Ocean Sea Salt in RO water). During the period under study here (0 to 2 dpf), the gender is not yet determined. The following mutant alleles were used: *cxcr4b*^{t26035} contains a nonsense mutation that results in a premature stop codon [26], *cxcr4a*^{um21} contains a 29 nt deletion and 4 nt insertion [27], *cxcl12a*^{30516} contains a nonsense mutation resulting in a premature stop codon [28], and *ackr3b*^{sa16} contains a nonsense mutation resulting in a premature stop codon [29]. The *TgBAC(cxcr4b:cxcr4b-Kate2-IRES-EGFP-CaaX-p7)* transgenic line expresses Cxcr4b fused to the monomeric red fluorescent protein Kate2 from the *cxcr4b* promoter and membrane-tethered GFP from an internal ribosome entry site (IRES) [9]. The *TgBAC(cxcr4b:cxcr4b-EGFP-IRES-Kate2-CaaX-p7)* transgenic line expresses Cxcr4b fused to GFP from the *cxcr4b* promoter and membrane-tethered Kate2 from an internal ribosome entry site (IRES) [9]. The *Tg(hsp70:cxcl12a)* transgenic line contains *cxcl12a* driven by the zebrafish heatshock promoter [30]. The *Tg(cldnB:lyn2GFP)* transgenic line contains an 8 kb fragment upstream of the *cldnb* start codon fused to a membrane-tethered GFP [31]. The *Tg(prim:lyn*$_2$*mCherry)* transgenic line contains a 7.2 kb fragment upstream of the *sox10* start codon fused to a membrane-tethered mCherry. This transgenic line does not recapitulate the *sox10* expression pattern but labels the posterior lateral line primordium among other structures [32]. The *TgBAC(cxcr4b:H2A-GFP)* transgenic line labels the nucleus of *cxcr4b*-expressing cells with GFP [33].

Generation of transgenic strains

All bacterial artificial chromosome (BAC) clones were verified by sequencing modified regions and EcoRI fingerprinting digest. The BAC DNA was isolated and purified with the NucleoBond BAC 100 kit (Clonetech) and co-injected with 40 ng/μl *tol2* mRNA into one-cell staged embryos. Stable transgenic animals were identified after out-crossing injected adults and screening for expression (*ackr3b:ackr3b-GFP*), GFP expression in the lens from the *cryaa*-driven transgenesis marker (*ackr3b:sfGFP, ackr3b:ackr3b*$^{wt\ tail}$*-sfGFP, ackr3b:ackr3b*$^{ST/A\ tail}$*-sfGFP, ackr3b:ackr3b*$^{K/A\ tail}$*-sfGFP*), and mScarlet, an RFP, expression in the myocardium from the *myl7*-driven transgenesis marker (*cxcr4b:Cerulean-CaaX, cxcr4b:cxcr4b-Citrine, cxcr4b:CXCR4-Kate2, cxcr4b:cxcr4b*$^{I7E,\ I8E}$*-Kate2-IRES-EGFP-CaaX)*).

For the *ackr3b:ackr3b-GFP* transgene, the BAC clone CH73–180E13 (Children's Hospital Oakland Research Center, CA, USA https://bacpacresources.org/) was modified twice by recombineering. First, *tol2* sites were inserted into the BAC backbone. Second, a targeting cassette containing the *GFP* coding sequence was inserted at the end of the *ackr3b* coding sequence. The BAC clone CH73–180E13 contains a 137 kb genomic DNA fragment that spans the *ackr3b* locus. Note that the this line does not express GFP from the *cryaa* promoter due to a deletion in the GFP coding sequence.

For the *ackr3b:sfGFP* transgene, the BAC clone CH73–180E13 was modified twice by recombineering. First, the targeting cassette *pBS-TarHom-Tol2-FRT-GalK-cryaa-sfGFP* was inserted into the BAC backbone. This adds *tol2* sites to facilitate transgenesis and a marker to identify transgenic animals [34]. Second, a targeting cassette containing *sfGFP* flanked by

630 bp homology arms upstream and 777 bp downstream of the coding sequence of *ackr3b* was inserted which replaced the coding sequence of *ackr3b* with sfGFP.

For the *ackr3b:ackr3b$^{wt\ tail}$-sfGFP* transgenic lines, the BAC clone CH73–180E13 was modified three times by recombineering. First the targeting cassette *pBS-TarHom-Tol2-FRT-GalK-cryaa-sfGFP* was inserted into the BAC backbone. Second, a targeting cassette containing a kanamycin resistance cassette (*kanR*) replaced exon 2 of *ackr3b* in the BAC along with 101 bp of upstream and 106 bp of downstream intronic sequences. This *kanR* replacement is necessary to create unique homology arms for the third targeting cassette to be introduced. Third, the *kanR* cassette was replaced with a targeting cassette containing *loxP-ackr3b-sfGFP-stop-loxP-ackr3b$^{ST/A\ tail}$-sfGFP-stop-FRT-GalK-FRT* or *loxP-ackr3b-sfGFP-stop-loxP-ackr3b$^{K/A\ tail}$-sfGFP-stop-FRT-GalK-FRT*. The intronic sequences which were originally replaced by *kanR* cassette in the second step are now reintroduced. The first *loxP* site is followed by 101 bp of intronic sequence upstream of exon 2 of *ackr3b* gene. The entire *ackr3b* exon 2 is duplicated with sfGFP-stop inserted at the end of the coding sequence of *ackr3b*. This is followed by 106 bp of intronic sequence downstream of exon 2 and a second *loxP* site. The second *ackr3b-sfGFP-stop* is duplicated with ST/A or K/A substitutions in the cytoplasmic tail followed by a FRT site. The *GalK* cassette was removed by flippase-mediated recombination. 24 bp of the end of exon 2 and 106 bp of intron after exon 2 are also duplicated. The full names of these transgenic lines are *Tg(ackr3b:loxP-ackr3b$^{wt\ tail}$-sfGFP-stop-loxP-ackr3b$^{ST/A\ tail}$-sfGFP)p4* and *Tg(ackr3b:loxP-ackr3b$^{wt\ tail}$-sfGFP-stop-loxP-ackr3b$^{K/A\ tail}$-sfGFP)p3*.

The *ackr3b:ackr3b$^{ST/A\ tail}$-sfGFP* and *ackr3b:ackr3b$^{K/Atail}$-sfGFP* transgenic lines were generated by injecting 8 pg *cre* mRNA into one-cell staged embryos from the corresponding *ackr3b:loxP-ackr3b$^{wt\ tail}$-sfGFP-stop-loxP-ackr3b$^{ST/A\ tail}$-sfGFP* and *ackr3b:loxP-ackr3b$^{wt\ tail}$-sfGFP-stop-loxP-ackr3b$^{K/A\ tail}$-sfGFP* transgenic lines. Transgenic animals were identified after out-crossing injected adults and sequencing the cytoplasmic tail. The offsprings were raised to generate stable transgenic lines which can be compared to their respective *ackr3b* wildtype tail founder lines because the BAC is integrated at the same location in the genome. The full names of these transgenic lines are *Tg(ackr3b:loxP-ackr3b$^{ST/A\ tail}$-sfGFP)p4* and *Tg(ackr3b:loxP-ackr3b$^{K/A\ tail}$-sfGFP)p3*.

For the following *cxcr4b* transgenes, the BAC clone DKEY169F10 (ImaGenes GmbH, Germany, sales@imagenes-bio.de) was first modified by inserting the targeting cassette *pIndigo-356-Tol2-kanR-myl7-mScarlet* into the BAC backbone through recombineering [34,35]. This modification adds *tol2* sites and the myocardium-specific transgenesis marker to the transgene. The BAC clone DKEY169F10 contains a 67 kb genomic DNA fragment that spans the *cxcr4b* locus.

For the cxcr4b:cerulean-CaaX transgene, a targeting cassette containing *cerulean-CaaX-FRT-GalK-FRT* flanked by homology arms 413bp upstream of *cxcr4b* exon2 and 420bp downstream of *cxcr4b* stop codon was inserted to replace the *cxcr4b* coding sequence in exon 2 (amino acid 6–358, the last amino acid before the stop codon). The *GalK* cassette was removed by flippase-mediated recombination. This transgene expresses the first five

amino acids from *cxcr4b* exon 1 fused to Cerulean-CaaX from the *cxcr4b* promoter. The full name of this transgenic line is *Tg(cxcr4b:cerulean-CaaX)p3*.

For the *cxcr4b:cxcr4b-citrine* transgene, a targeting cassette containing *citrine-FRT-GalK-FRT* flanked by homology arms 583 bp upstream and 433 bp downstream of the *cxcr4b* stop codon was inserted to tag the *cxcr4b* coding sequence in exon 2 with citrine. The *GalK* cassette was removed by flippase-mediated recombination. This transgene expresses zebrafish Cxcr4b fused to citrine from the *cxcr4b* promoter. The full name of this transgenic line is *Tg(cxcr4b:cxcr4b-citrine)p2*.

For the *cxcr4b:CXCR4-Kate2* transgene, a targeting cassette containing the coding sequence for the first five amino acids (MEGIS) of human *CXCR4* fused to *GalK* flanked by homology arms 429bp upstream of the *cxcr4b* start codon and 345bp downstream of *cxcr4b* exon 1 was inserted to replace the coding sequence for the first five amino acids of zebrafish *cxcr4b* in exon 1. The GalK sequence was removed by seamless recombineering using a PCR template identical to the one described above but lacking the GalK sequence. Next, a targeting cassette containing *human CXCR4 (coding nucleotides 16–1056)-Kate2-FRT-GalK-FRT* flanked by homology arms 413 bp upstream and 433 bp downstream of the coding sequence for *cxcr4b* in exon 2 replaced the coding sequence of zebrafish *cxcr4b* in exon 2 with the coding sequence of human *CXCR4* (codons 6–352) fused to *Kate2*. The *GalK* cassette was removed by flippase-mediated recombination. This transgene expresses human CXCR4 fused to Kate2 from the *cxcr4b* promoter. The full name of this transgenic line is *Tg(cxcr4b:CXCR4-Kate2)p2*.

For the *cxcr4b:cxcr4b*^{I7E,I8E}*-Kate2-IRES-eGFP-CaaX* transgene, a targeting cassette containing *cxcr4b*^{I7E,I8E}*-Kate2-IRES-eGFP-CaaX-FRT-GalK-FRT* flanked by homology arms 46 bp upstream of exon 1 of *cxcr4b* and 433 bp downstream of the *cxcr4b* stop codon was inserted to replace the human CXCR4 coding sequence in exon 1 and exon 2 of the *cxcr4b:CXCR4* BAC transgene. The *GalK* cassette was removed by flippase-mediated recombination. This transgene expresses zebrafish Cxcr4b with isoleucines at position 7 and 8 of the N-terminus replaced with two glutamates fused to Kate2 from the *cxcr4b* promoter. Also, this transgene expresses membrane-tethered GFP-CaaX from an internal ribosomal entry site (IRES) from the same transcript. The full names of these transgenic lines are *Tg(cxcr4b:cxcr4b*^{I7E,I8E}*-Kate2-IRES-eGFP-CaaX)p8, p9* and *p10*. The three different lines were used interchangeably in this study.

Genotyping of ackr3b$^{wt\ tail}$-sfGFP and ackr3b$^{ST\ and\ K/A\ tail}$-sfGFP transgenic lines

Outer: ACCCAGTGGAAAGCATGAAGGAGT and GGTCAACACCATTAAAGAAAGTTCACTTGTACAGCTCGTCCATGC

Inner: CATGCTTGGCTTTGCCATTC and GCTCCTCGCCCTTGCTCACCAT

PCR amplicons were sequenced with: CATGCTTGGCTTTGCCATTC

Generation of zebrafish and human Cxcl12-signaling sensor cell lines

Zebrafish *cxcr4b-Kate2-IRES-GFPF* and human *CXCR4-Kate2-IRES-GFPF* was subcloned from *pCS2-cxcr4b-Kate2-IRES-GFPF* and *pCDNA3.1+-CXCR4-Kate2-IRES-GFPF*, respectively, [9] into *pCDNA5/FRT/TO* (Thermo Fisher Scientific, catalog number V652020) to generate *pCDNA5/FRT/TO-cxcr4b-Kate2-IRES-GFPF* and *pCDNA5/FRT/TO-CXCR4-Kate2-IRES-GFPF*. 1.5 μg of the plasmid and 13.5 μg of *pOG44* Flp-recombinase expression vector (Thermo Fisher Scientific, catalog number V600520) were co-transfected into a 30 % confluent 10 cm plate of T-REx HEK 293 cells (Thermo Fisher Scientific, catalog number A15008) using Lipofectamine 2000 (Thermo Fisher Scientific, catalog number 11668027). Both cell lines were re-plated onto 15 cm plates in DMEM + 10% FBS + 100 μg/mL hygromycin + 15 μg/mL blasticidin and maintained in selection media for two weeks to select for clones with stably integrated constructs. Colonies that emerged after two weeks were transferred into 24-well plates using cloning cylinders and expanded. Cells were grown in DMEM (Thermo Fisher Scientific, catalogue number 10–013-CV), 1 % glucose (Gibco, catalog number A2494001), 1 % penicillin-streptomycin (Gibco, catalog number 15140122), and 5 % FBS (Gibco, catalog number 10099). Early passage clones were frozen. Clones were analyzed for expression of Kate2 and GFPF by live confocal microscopy following doxycycline induction, and clones with uniform GFP and RFP expression were used for further experiments (Fi4b#5 and Hu4#11). Note that the cell lines carry a single copy of the Cxcl12-signaling sensor at the genomic FRT site under the control of the tetracycline-inducible hybrid human cytomegalovirus (CMV)/TetO2 promoter.

Generation of zebrafish *cxcr4b*^{I7E,I8E} cell line

The plasmid *pCDNA5/FRT/TO-cxcr4b*^{I7E,I8E}*-Kate2-IRES-GFPF* was generated from the plasmid *pCDNA5/FRT/TO-cxcr4b-Kate2-IRES-GFPF* (see above) using Gibson cloning. The primer 5’-GGTGGAATTCATGGAATTTTACGATAGCGAAGAATTAGACAACAGCTCTGACTCC-3’ was used to mutate the codons for isoleucines 7 and 8 to codons for glutamates. 0.4 μg of the plasmid and 3.6 μg of *pOG44* Flp-recombinase expression vector (Thermo Fisher Scientific, catalog number V600520) were co-transfected into a 30 % confluent 6-well plate of T-REx HEK 293 cells (Thermo Fisher Scientific, catalog number A15008) using Lipofectamine 2000 (Thermo Fisher Scientific, catalog number 11668027). The cell line was re-plated onto 10 cm plates in DMEM + 10% FBS + 100 μg/mL hygromycin + 15 μg/mL blasticidin and maintained in selection media for 10 days to select for clones with stably integrated constructs. Colonies that emerged after 10 days were transferred into 96-well plates using cloning cylinders and expanded. Early passage clones were frozen. Clones were analyzed for expression of Kate2 and GFPF by live confocal microscopy following doxycycline induction, and tested for sensitivity to 1mg/mL zeocin.

Generation of recombinant zebrafish Cxcl12a

The coding sequence of zebrafish *cxcl12a* was cloned into the *pET28a-His6-Sumo* to generate *pET28a-His6-Sumo-cxcl12a*. The *pET28a-His6-Sumo-cxcl12a* plasmid was transformed into *E.coli* strain BL21 (DE3) (New England Biolabs, catalogue number C2527l) and grown in LB with 25 μg/mL kanamycin (Millipore Sigma, catalogue number

60615) at 37 degree Celsius. Cxcl12a protein expression was induced by addition of IPTG (Millipore Sigma, catalogue number I6758) to a final concentration of 1 mM when the bacteria culture reached an OD600 of 0.5. After 6 hours of growth the bacteria culture was spun at 6000 rpm for 15 minutes. Pellets were stored at −80 degrees Celsius until further processing. Cell pellets were resuspended in 10 mL of suspension buffer (50 mM Na_2PO_4 pH 8.0, 300 mM NaCl, 10 mM imidazole, 1 mM phenylmethylsufonyl fluoride, and 1 mM DTT). Cells were lysed by sonication on ice. Triton was added to 0.2 % final volume fraction and cultures were nutated for 15 minutes at 4 degrees Celsius. Then, lysates were spun at 10,000 g for 30 minutes at 4 degrees Celsius and the supernatant was discarded. Pellets were resuspended and solubilized with buffer AD (50 mM sodium phosphate pH 7.4, 300 mM NaCl, 10 mM imidazole, 6 M guanidinium hydrochloride, 1 mM DTT and 50 mmol/L phenylmethylsufonyl fluoride). The solution of the dissolved pellet was loaded onto Ni-NTA resin (Qiagen, catalogue number 30210) for affinity purification of the overexpressed His-Sumo-Cxcl12a protein. After 30 min incubation at room temperature, the column was washed with buffer AD, and the His-Sumo-Cxcl12a protein was eluted off the column using an elution buffer (50 mmol/L sodium acetate pH 4.5, 300 mmol/L NaCl and 10 mmol/L imidazole). Eluates containing protein were identified by Bradford dye binding assay (Bio-Rad, Protein Assay Kit I, catalogue number #5000001) and pooled. His-Sumo-Cxcl12a protein was refolded by a drop-wise dilution into folding buffer (20 mM Tris pH 8.0, 10 mM cysteine, and 0.5 mM cystine solution). Following overnight incubation at 4 degrees Celsius the solution was concentrated first by ammonium sulfate precipitation, followed by ultrafiltration using Vivaspin 20 with a 10,000 molecular weight cut-off columns (Sartorius, catalogue number VS2001). Protein was dialyzed against Ulp1 protease buffer (50 mM Tris-HCl, pH 8.0, 0.2 % Igepal (NP-40), 0.15 M NaCl and 1 mM DTT) overnight followed by incubation with Ulp1 protease (Thermo Fisher Scientific, catalogue number 12588018) for 12 hours at 30 degrees Celsius. Samples were then loaded onto SP Sepharose Fast Flow (GE Healthcare, catalogue number 17072901) resin and the column was washed with wash buffer (50 mM Tris pH 8.0, 50 mM NaCl) to remove the His-Sumo-tag. Cxcl12a (and uncleaved His-Sumo-Cxcl12a) protein was eluted with 20 mM Tris pH 8.0 containing 2 M NaCl. Lastly, samples were purified to more than 98% homogeneity using reverse-phase high-performance liquid chromatography with a 30 minute gradient from 30 % to 60 % acetonitrile in aqueous 0.1 % trifluoroacetic acid. Cxcl12a protein was frozen, lyophilized and stored at −20 degrees Celsius. Working concentrations of Cxcl12a protein were rehydrated in Phosphate-Buffered Saline, pH 7.4 (ThermoFischer Scientific, catalogue number 10010023) and diluted to the appropriate concentrations in cell culture media.

Live Imaging

All confocal images were collected in photon counting mode on a Leica SP5 II or Leica SP8 confocal microscope with HyD detectors and a heated stage (Warner Instruments LLC, USA). The laser power was calibrated before each imaging session using an X-Cite Power Meter Model XR2100 (Lumen Dynamics), which measures the power of laser light emitted from the objective onto the stage. All embryos were mounted in 0.5 % low-melt agarose dissolved in fish water supplemented with 0.4 mg/ml MS-222 anesthetic (Sigma, catalogue number E10521) and imaged around 36 hpf unless otherwise noted.

Live imaging of Cxcl12a-Signaling Sensor Embryos and Cultured Cells—Wild-type or *cxcl12a* mutant embryos transgenic for *cxcr4b:cxcr4b-Kate2-IRES-EGFP-CaaX* were mounted together in a 35 mm dish. Similarly, *cxcr4b:cxcr4b-Kate2-IRES-EGFP-CaaX* transgenic embryos with or without *hsp70:cxcl12a* transgene were mounted together in a 35 mm dish. For embryos overexpressing Cxcl12a, embryos were heat shocked for 30 min at 39.5 degrees Celsius before imaging. For cultured cells, cells were induced with 1 μg/mL doxycycline (Sigma Aldrich, catalogue number D9891) for 24 hours before addition of purified Cxcl12a. Cells were grown on single or 6-well 35 × 10 mm plates to about 50–90 % confluency at time of imaging. One hour before imaging, the media was replaced with dilutions of Cxcl12a in DMEM lacking phenol red (Gibco, catalogue number 21063–029). Images were acquired using the Leica SP5 II confocal microscope or a Leica SP8 confocal microscope and a Leica 40x NA 0.8 water dipping objective (HCX APO L 40x/0.80 W U-V-I). Four frame accumulations and Z-stacks of 1.05 μm section thickness were collected. The 488 nm laser power was set at 300 μW and 561nm laser power set to 1mW using an X-Cite Power Meter Model XR2100 (Lumen Dynamics).

Live imaging of transgenic Ackr3b and Ackr3b transcriptional reporter embryos—The *ackr3b:ackr3b-GFP; prim:lyn$_2$mCherry* embryos in *cxcr4a$^{-/-}$; cxcr4b$^{-/-}$* or wild-type background with and without the *hsp70:cxcl12a* transgene were mounted together on a 35 mm petri dish. The dish was submerged in water and heat-shocked at 39.5 degrees C for 30 minutes. Within 1–2 hours after the end of the heat shock, the primordium of each embryo was imaged every hour for 7–10 hours. Images were acquired using the Leica SP5 II confocal microscope and a Leica 40x NA 0.8 water dipping objective (HCX APO L 40x/0.80 W U-V-I). Four frame accumulations and Z-stacks of 1.05 μm section thickness were collected. The 488 nm laser power was set at 300 μW.

The *ackr3b:sfGFP; prim:lyn$_2$mCherry* embryos with and without *hsp70:cxcl12a* transgene were imaged the same as above.

The *ackr3b:ackr3b$^{wt\ tail}$-sfGFP; ackr3b$^{-/-}$; prim:lyn$_2$mCherry* and *ackr3b:ackr3b$^{ST/A\ tail}$-sfGFP; ackr3b$^{-/-}$; prim:lyn$_2$mCherry* embryos with and without *hsp70:cxcl12a transgene* were imaged the same as above but using the Leica SP8 confocal microscope.

The *ackr3b:ackr3b$^{wt\ tail}$-sfGFP; ackr3b$^{-/-}$; prim:lyn$_2$mCherry* and *ackr3b:ackr3b$^{K/A\ tail}$-sfGFP; ackr3b$^{-/-}$; prim:lyn$_2$mCherry* embryos with and without *hsp70:cxcl12a* transgene were imaged the same as *ackr3b:ackr3b$^{wt\ tail}$-sfGFP; ackr3b$^{-/-}$; prim:lyn$_2$mCherry* and *ackr3b:ackr3b$^{ST/A\ tail}$-sfGFP; ackr3b$^{-/-}$; prim:lyn$_2$mCherry* embryos.

The expression of *ackr3b:ackr3b$^{wt\ tail}$-sfGFP; ackr3b$^{-/-}$; prim:lyn$_2$mCherry* and *ackr3b:ackr3b$^{ST/A\ tail}$-sfGFP; ackr3b$^{-/-}$; prim:lyn$_2$mCherry* embryos were imaged using the Leica SP8 confocal microscope with a Leica 40x NA 1.1 water immersion objective (HC PL APO 40x/1.10 W CORR CS2). The pinhole was set at 2 Airy units. Four frame accumulations and Z-stacks of 1.01 μm were collected. The 488 laser power was set at 300 μW.

The expression of *ackr3b:ackr3b$^{wt\ tail}$-sfGFP; ackr3b$^{-/-}$; prim:lyn$_2$mCherry* and *ackr3b:ackr3b$^{K/A\ tail}$-sfGFP; ackr3b$^{-/-}$; prim:lyn$_2$mCherry* embryos were imaged the same as above but with a Leica SP5 confocal microscope.

The migration of *ackr3b:ackr3b$^{wt\ tail}$-sfGFP; prim:lyn$_2$mCherry*, *ackr3b:ackr3b$^{ST/A\ tail}$-sfGFP; ackr3b$^{-/-}$; prim:lyn$_2$mCherry, and ackr3b$^{-/-}$; prim:lyn$_2$mCherry* embryos were imaged using a Leica SP8 confocal microscope with a Leica 20x NA 0.5 water dipping objective (HCX APO L 20x/0.50 W U-V-I). The pinhole was set at 2 Airy units. Two frame accumulations and Z-stacks of 2.64 μm section thickness were collected.. Embryos were mounted together on a 35mm petri dish and imaged every 10 minutes for 15 hours.

Live imaging of transgenic Cxcr4b embryos—The *cxcr4b:cxcr4b-Citrine*; *cxcr4b:Cerulean-CaaX* line and the *cxcr4b:CXCR4-Kate2*; *cxcr4b:Cerulean-CaaX* line were imaged using the Leica SP8 confocal microscope and a Leica 40x NA 1.1 water immersion objective (HC PL APO 40x/1.10 W CORR CS2). The pinhole was set to 177 nm. The 514 nm laser was set to 30 μW, the 458 nm laser was set to 9 μW and the 561 nm laser was set to 65 μW.

The *cxcr4b:cxcr4b-Kate2-IRES-eGFP-CaaX; cldnb:lyn$_2$GFP* and *cxcr4b:CXCR4-Kate2; cldnb:lyn$_2$GFP* embryos with and without the *hsp70:cxcl12a* transgene were mounted together on a 35 mm petri dish. The dish was submerged in water and heat-shocked at 39.5 degrees C for 10 minutes. 15 minutes after the end of the heat shock, the primordium of each embryo was imaged every 15 minutes for 14.5 hours. Images were acquired using the Leica SP8 confocal microscope and a Leica 40x NA 0.8 water dipping objective (HCX APO L 40x/0.80 W U-V-I). The pinhole was set at 2 Airy units. Two frame accumulations and Z-stacks of 2.1 μm section thickness were collected.

The migration of *cxcr4b:cxcr4b-Citrine; cldnb:lyn$_2$GFP* and *cxcr4b:CXCR4-Kate2; cldnb:lyn$_2$GFP* embryo movies were imaged using the Leica SP8 confocal microscope with a Leica 20x NA 0.5 water dipping objective (HCX APO L 20x/0.50 W U-V-I). The pinhole was set at 2 Airy units. Two frame accumulations and Z-stacks of 2.64 μm section thickness were collected. Embryos were mounted together on a 35 mm petri dish and imaged every 10 minutes for 13 hours.

The front of the primordia of *cxcr4b:CXCR4-Kate2; cxcr4b$^{-/-}$; cldnb:lyn$_2$GFP* and *cxcr4b$^{-/+}$; cldnb:lyn$_2$GFP* embryos were collected using the Leica SP8 confocal microscope with a Leica 40x NA 1.1 water immersion objective (HC PL APO 40x/1.10 W CORR CS2). The pinhole was set at 1 Airy units. Four frame accumulations and Z-stacks of 1 μm section thickness were collected every 2 minutes for 1 hour.

The *cxcr4b:cxcr4b-Kate2-IRES-eGFP-CaaX* and the *cxcr4b:cxcr4b^{I7E,I8E}-Kate2-IRES-eGFP-CaaX* line were imaged using the Leica SP8 confocal microscope and a Leica 40x NA 1.1 water immersion objective (HC PL APO 40x/1.10 W CORR CS2). The pinhole was set to 1 Airy units. Four frame accumalations and Z-stacks of 1.01μm section thickness were collected. The 488 nm laser was set to 300 μW and the 561 nm laser was set to 1 mW.

Live imaging of transgenic Ackr3b and Cxcr4b embryos—The *cxcr4b:cxcr4b-eGFP-IRES-Kate2-CaaX* and *ackr3b:ackr3b$^{wt\ tail}$-sfGFP; ackr3b$^{-/-}$; prim:lyn$_2$mCherry* embryos with and without the *hsp70:cxcl12a* transgene were mounted together on a 35 mm petri dish. The dish was submerged in water and heat-shocked at 39.5 degrees C for 10 minutes. 10 minutes after the end of the heat shock, the primordium of each embryo was imaged every 10 minutes for 12hours. Images were acquired using the Leica SP8 confocal microscope and a Leica 40x NA 0.8 water dipping objective (HCX APO L 40x/0.80 W U-V-I). The pinhole was set at 2 Airy units. Two frame accumulations and Z-stacks of 3 μm section thickness were collected.

Nuclear tracking of primordium cells—*cxcr4b:CXCR4-Kate2; cxcr4b$^{-/-}$; cxcr4b:H2A-GFP* and *cxcr4b:Cxcr4b-Citrine; cxcr4b$^{-/-}$; cxcr4b:H2A-GFP*/*cxcr4b:Cxcr4b-Citrine; cxcr4b$^{-/+}$; cxcr4b:H2A-GFP* embryos were mounted together on a 35 mm petri dish and imaged with a Nikon Ti2-E/CSU-W1 spinning disc equipped with IXON LIFE 888 EMCCD cameras using a 40X water objective (Nikon CFI APO LWD 40X WI 1.15 NA LAMBDA S). Z-stacks of 1 μm section thickness were collected every 2 minutes for 2 hours. The time lapse videos were imported onto Imaris Version 7.0 (Bitplane, Oxford Instruments), and the Spots tool with a specified cell diameter of 3.75 μm, default background subtraction, and quality above automatic threshold was used to detect the cell nuclei in the primordium. The cell nuclei were tracked using the autoregressive motion algorithm with a maximum distance that an object can move between two consecutive time points set to 20 μm and a maximum gap size that an object is allowed to be missing in order to join track fragments set to two. After running the tracking algorithm, the tracks of the first ten to eleven leader cell nuclei in the front of the primordium were manually curated to correct track segments and remove dying cells. For dividing cells, the daughter cell that was closer to the front of the primordium was tracked. All the x, y, z, t and track IDs were exported. This yielded a set of vectors in three-dimensional space where the vector Pt denotes the xyz-coordinates of each cell nucleus at time point t. This data set was used to calculate the directional angles, average speed, directionality indices, and neighbor-neighbor distances using MatLab scripts (Supplementary Data 7) as described [36].

Quantification of the Cxcl12a-Signaling Sensor in embryos

To calculate the ratio of Kate2/GFP on the membrane of the primordium, a custom ImageJ (NIH) macro language script (Supplementary Data 3) was written to divide the Kate2 channel by the GFP channel and then multiply the ratio image to a membrane mask. The membrane mask was generated by thresholding the GFP channel. Background values from the membrane Kate2 to GFP ratio image were removed by setting a threshold of 0.02. All values from the ratio image stacks were saved as a text file. A custom python script (Supplementary Data 4) was written to calculate the mean, standard deviation, and number of values across the dorsal-ventral and anterior-posterior axis of the primordia of all the embryos imaged. For averaging across embryos with identical genotype, the front of the primordium in each Z-stack was assigned to the 0 μm position. Wild-type embryos were plotted along the first 150μm of the anterior-posterior axis of the primordium. A shorter length of 100 μm or 30 μm were used for embryos overexpressing Cxcl12a or lacking

Cxcl12a, respectively, because the primordium frequently rounds up and becomes shorter than 150 μm.

Quantification of the Cxcl12-Signaling Sensors in cultured cells

To calculate the ratio of Kate2/GFP on the membrane of cultured cells, a custom ImageJ script (Supplementary Data 1) was written to extract the Kate2 and GFP values on the cell membrane before calculating the red-to-green ratio. First, a membrane mask was generated for each z-stack by smoothening the GFP channel using a Gaussian blur of radius 1.5, followed by determining local maxima using the Find Maxima function with a noise tolerance of 1.3. The membrane mask was converted into a binary image and multiplied to the Kate2 and GFP channels. All values in the Kate2 and GFP channels outside of the mask were discarded and outliers were removed by thresholding. A high threshold for membrane Kate2 values greater than 2 times the mean RFP intensity was applied. A low threshold for membrane GFP values less than 13 was applied to remove background signal, and a high threshold of greater than 4.5 times the mean GFP intensity was applied. The thresholded membrane Kate2 and GFP values were divided by each other to generate a ratio image. Text images representing all of the membrane Kate2/GFP values were created from the ratio image. For each experimental condition, text images were pooled together and the mean, standard deviation, and number of values were computed using a custom python script (Supplementary Data 2).

Quantification of Ackr3b and Ackr3b transcriptional reporter intensity

A custom ImageJ script (Supplementary Data 8) was written to calculate the GFP intensities in the primordia. First, a total mask of the primordia was generated using the RFP channel. The mask was generated using the Huang threshold algorithm and filling holes, eroding, and dilating to create the best fitted mask encompassing the primordia. The mask was made into a binary image and multiplied to the RFP channel. A minimum threshold of 2 was used to remove background intensity. All values from the image stacks were saved as a text file and a custom python script (Supplementary Data 4) was written to calculate the mean, standard deviation, and number of values across the dorsal-ventral and anterior-posterior axis of the primordia of all the embryos imaged. For averaging across embryos with identical genotype, the front of the primordium in each Z-stack was assigned to the 0 μm position and plotted along the average length of the anterior-posterior axis of the primordia. A shorter length was used for embryos overexpressing Cxcl12a because the primordium rounds up and becomes shorter.

Quantification of Cxcr4b, Cxcr4b^{I7E,I8E}, and CXCR4 internalization across the primordium

A custom Image J script (Supplementary Data 5) was written to calculate the ratio of Cxcr4b-Citrine/Cerulean and CXCR4-Kate2/Cerulean on the membrane of the primordium. This script divides the Citrine and Kate2 channels by the Cerulean channel, respectively, and then multiplies the ratio images to a membrane mask. The membrane mask was generated by thresholding the Cerulean channel using the moment-preserving thresholding algorithm in ImageJ [37]. Background values from the membrane Citrine/Cerulean and Kate2/Cerulean ratio images were removed by setting a threshold of 0.02. All values from the ratio image stacks were saved as a text file. For averaging across embryos with identical genotype, the

front of the primordium in each Z-stack was assigned to the 0 μm position. The Citrine/Cerulean and Kate2/Cerulean ratios were then normalized to the average ratio in the back of the primordium (50 μm to 100 μm) for comparison. The normalized ratios of the embryos were plotted along the first 100 μm of the anterior-posterior axis of the primordium.

To calculate the ratio of Cxcr4b-Kate2 on the membrane and compare it to Cxcr4b^{I7E,I8E}-Kate2 on the membrane, the ImageJ (NIH) macro language script used for the Cxcl12a signaling sensor described above (Supplementary Data 3) was applied.

Note that membrane-bound CFP and the membrane-bound GFP are expressed from the *cxcr4b* promoter and the CFP and GFP fluorescence intensity are a measure of the total chemokine receptor production.

Quantification of Cxcr4b and CXCR4 internalization kinetics

A custom Image J Script (Supplementary Data 6) was written to calculate the RFP intensity on the membrane of the primordia for each time point post heat-shock. First, a membrane mask was generated using the GFP channel. Second, the RFP channel was multiplied by the membrane mask to extract all the RFP intensities on the membrane. Then the RFP intensities on the membrane were summed up and divided by the sum of the voxels of the membrane mask to normalize for the size of each primordia.

The RFP intensities on the primordium cell membranes of Cxcl12a-overexpressing embryos were normalized to the RFP intensities of primordium cell membranes in heat-shocked control embryos. To normalize, the RFP intensities in the primordia of the Cxcl12a-overexpressing embryos were divided by the average RFP intensities at each time point of the primordia of heat-shocked control embryos. For some time points no heat-shock control values were available because the primordia had migrated out of the imaging field. In these cases, the RFP intensities were divided by the average RFP intensities of all the time points in all the heat-shocked control embryos.

To calculate the half-lives, the internalization of Cxcr4b and CXCR4 were fitted to a one-exponential decay model ($y=(y_0 - y_{plateau})*\exp(-k*x) + y_{plateau}$) using the Levenberg-Marquardt method for non-linear regression in PRISM (Version 7.0e, GraphPad, Fig. 2d, Extended Data Fig. 2c).

To assess if the differences in zebrafish Cxcr4b-Kate2 and human CXCR4-Kate2 internalization kinetics are due to their different K_ds for Cxcl12a, we fitted the Cxcr4b-Kate2-to-CXCR4-Kate2 internalization ratio to the expected ratio for steady state receptor ligand binding ($[RL] = [R_{tot}]*[L]/(K_d+[L])$) of two receptor with a K_d of 3.4 nM and 782 nM using the following equation

$$\boldsymbol{y} = \boldsymbol{A}*(782 + \boldsymbol{B}*[\boldsymbol{L}])/(\boldsymbol{3.4} + \boldsymbol{B}*[\boldsymbol{L}])$$

where A corresponds to $R_{tot,\ fish}/R_{tot,\ human}$ and B is a scaling factor that converts time to Cxcl12a concentration with the assumption that the production rate of Cxcl12a is linear and Cxcl12a degradation negligible. The fit was performed using the Levenberg-Marquardt

method for non-linear regression in PRISM (Version 7.0e, GraphPad, Extended Data Fig. 2b and d).

Quantification of Cxcr4b and Ackr3b expression kinetics

Two custom Image J Script were written to calculate the total GFP intensities inside primordia for each time point post heat-shock for Cxcr4b-GFP (Supplementary Data 9) and Ackr3b-GFP (Supplementary Data 10). To extract Cxcr4b-GFP intensities, a mask was generated using the RFP channel. Then, the GFP channel was multiplied by this mask to extract the sum of the GFP intensities inside the primordium. To extract Ackr3b-GFP intensities, first a mask was generated using the RFP channel. Second, a mask was generated using the GFP channel. These two masks were combined using the logical operator 'AND'. Then, the GFP channel was multiplied by this combined mask to extract the sum of the GFP intensities inside the primordium.

To estimate the initial rates of intensity change, the time points 50 min to 90 min post heat shock were fitted to a linear equation (y = ax + b) using linear regression in PRISM (Version 7.0e, GraphPad, Extended Data Fig. 4c, d).

Calculation of the Cxcl12-Cxcr4 dissociation constants and maximal binding constants

We measured the FmemRed/FmemGreen ratio of HEK 293 cells (K/G_{cells}) expressing the zebrafish or human Cxcl12-signaling sensors exposed to increasing zebrafish and human Cxcl12 concentrations as described above. We normalized the mean K/G_{cells} by subtracting the mean K/G_{cells} in cells not exposed to Cxcl12.

$$K/G_{cells}^{norm} = K/G_{cells}([Cxcl12] = 0) - K/G_{cells}([Cxcl12])$$

The normalized K/G_{cells} was plotted against the increasing concentrations of Cxcl12. To determine the dissociation constants (K_d) and maximal binding constants (B_{max}), the data were fitted to a one site specific binding model using the Levenberg-Marquardt method for non-linear regression in PRISM (Version 7.0e, GraphPad, Fig. 1h, Extended Data Fig. 1d–f, Extended Data Fig. 3b).

$$K/G_{cells}^{norm} = B_{max}^{cells} * [Cxcl12]/(K_d + [Cxcl12])$$

Calculation of the signaling-available Cxcl12a concentration in the embryo

The equation describing monovalent ligand-receptor binding at equilibrium for an excess of ligand (the free ligand concentration is close to the total ligand concentration) is:

$$[C]_{eq} = [R]_t * [L]_t/(K_d + [L]_t)$$

where $[C]_{eq}$ is the concentration of the receptor-ligand complex at equilibrium, $[R]_t$ is the total receptor concentration, $[L]_t$ is the total ligand concentration and K_d is the dissociation

constant [38]. This equation can be rearranged to express how the ligand concentration depends on the ligand-receptor complex concentration:

$$[L]_t = [C]_{eq} * K_d / ([R]_t - [C]_{eq})$$

Since the normalized K/G_{cells} is proportional to $[C]_{eq}$, B_{max} is proportional to $[R]_t$, and $[L]_t$ corresponds to [Cxcl12a] this equation can be rewritten as:

$$[Cxcl12a] = K_d * K/G^{norm}_{cells} / (B^{cells}_{max} - K/G^{norm}_{cells})$$

The B_{max} in cultured cells and embryos is different (Fig. 1g, h). To adjust for this, we measured the K/G_{fish} in the primordium of *cxcl12a*$^{-/-}$ embryos and embryos overexpressing Cxcl12a from a heat shock promoter. These genetic scenarios correspond to embryos in which the primordia are exposed to no Cxcl12a ([Cxcl12a] = 0) and to saturating Cxcl12a concentrations, respectively. Since the primordium is rounded in *cxcl12a*$^{-/-}$ embryos and in embryos overexpressing Cxcl12a, we calculated the mean K/G_{fish} across the first 5 to 30 μm in *cxcl12a*$^{-/-}$ primordia and the first 5 to 100 μm in Cxcl12a-overexpressing primordia. The effect of the heat shock on K/G_{fish} in the primordium was accounted for by measuring the K/G_{fish} in non-heat-shocked and heat-shocked wild-type primordia. This was used to calculate a correction factor f_{temp} for each K/G_{fish} ratio along the front-back axis of the primordium.

$$f_{temp} = K/G^{28C}_{fish} / K/G^{39C}_{fish}$$

The f_{temp} correction factors for each position along the front-back axis of the primordium were then used to correct the K/G_{fish} of the primordia in heat-shocked *hsp70:cxcl12a* embryos for the heat shock effect. The difference between the K/G_{fish} in primordia lacking or overexpressing Cxcl12a was used to determine the B_{max} in the embryo. We used the correction factor f to convert the B_{max} in cells to the B_{max} in the embryo:

$$f = B^{cells}_{max} / B^{fish}_{max}$$

Incorporation of this correction factor into the equation above yields:

$$[Cxcl12a] = K_d * K/G^{norm}_{fish} * f / (B^{cells}_{max} - K/G^{norm}_{fish} * f)$$

We used this equation to calculate the signaling-available Cxcl12a concentration around the primordium.

Whole mount in situ hybridization

Preparation of RNA probes and whole mount *in situ* hybridization were performed as previously described [39]. Briefly, we cloned the *epcam* DNA template with the primers listed below using a zebrafish 36 hpf cDNA library generated from polyA RNA extracted with

Trizol (ThermoFisher, catalogue number: 15596018) and reverse transcribed with SuperScript III (ThermoFisher, catalogue number: 18080044). The *epcam* amplicon was cloned into pBluescript. The *epcam* probe was *in vitro* transcribed with digoxigenin-labelled nucleotides (Millipore Sigma, catalogue number: 11277073910). The probe was detected with anti-DIG-AP antibody (1:5000, Millipore Sigma, catalogue number: 11093274910) and NBT/BCIP (1:1000 each, Millipore Sigma, catalogue number: 11681451001). Embryos were fixed in 4% PFA (Millipore Sigma, catalogue number: P6148–500G) overnight at room temperature. Following fixation, they were permeabilized in methanol (Fisher Scientific, catalogue number: A413–500) at −20 degree C, rehydrated, permeabilized with 10 mg/ml proteinase K (Millipore Sigma, catalogue number: P2308–5MG) in PBST for 8 minutes at room temperature, and post-fixed in 4% PFA for 20 minutes at room temperature. Blocking and probe hybridization were performed at 68 degree C overnight. Following probe hybridization and washes, embryos were blocked in 2% BSA (Millipore Sigma, catalogue number: A8022–50G) in PBST and incubated with anti-DIG-AP antibody overnight at 4 degree C. Embryos were washed and developed in NBT/BCIP solution overnight at room temperature.

Epcam-EcoRI: ggccgaattcGTGGGCAAACTGTGATGACTCGT

Epcam-XhoI: ggccctcgagTCGCCGTGCAAGAAAGAACAG

Quantification of primordium migration distance

Embryos were imaged live between 48 and 49 hpf using a Leica M165 FC stereo microscope. Primordium migration distance was measured as the distance the primordium migrated divided by the distance to the tip of the tail. The values were then normalized to the average migration distance of wild-type embryos.

Statistics and reproducibility

Statistical analyses were performed using the Prism software (Versions 7.0e and 8.1.2, GraphPad) or the web interface estimationstats.com [40]. For Fig. 2d, the experiment was independently repeated once with similar results but different embryo numbers (n=3 embryos for Cxcr4b-Kate2 and n=4 embryos for CXCR4-Kate2) and the data are shown in Extended Data Fig. 2c and d. For Fig. 5d, the experiment was independently repeated once with similar results (n=4 embryos for *ackr3b*$^{-/-}$; *ackr3b:ackr3b*$^{wt\ tail}$*-sfGFP,* n=1 embryo for *ackr3b*$^{-/-}$; *hsp:cxcl12a*; *ackr3b:ackr3b*$^{wt\ tail}$*-sfGFP,* n=4 embryos for *ackr3b*$^{-/-}$; *ackr3b:ackr3b*$^{ST/A\ tail}$*-sfGFP,* and n=3 embryos for *ackr3b*$^{-/-}$; *hsp:cxcl12a*; *ackr3b:ackr3b*$^{ST/A\ tail}$*-sfGFP).* For Extended Data Fig. 4c and d, the experiment was independently repeated once with similar results (n=3 embryos for Cxcr4b-GFP, n=1 embryo for Cxcr7b-sfGFP).

Code availability

All codes are provided as Supplementary Data 1 to 10.

Data availability

Source data for Figures 1 to 5 and Supplementary Figures 1 to 5 have been provided as Source data files. The modeling data have been provided in Supplementary Table 3. All other data supporting the findings of this study are available from the corresponding author on reasonable request.

Extended Data

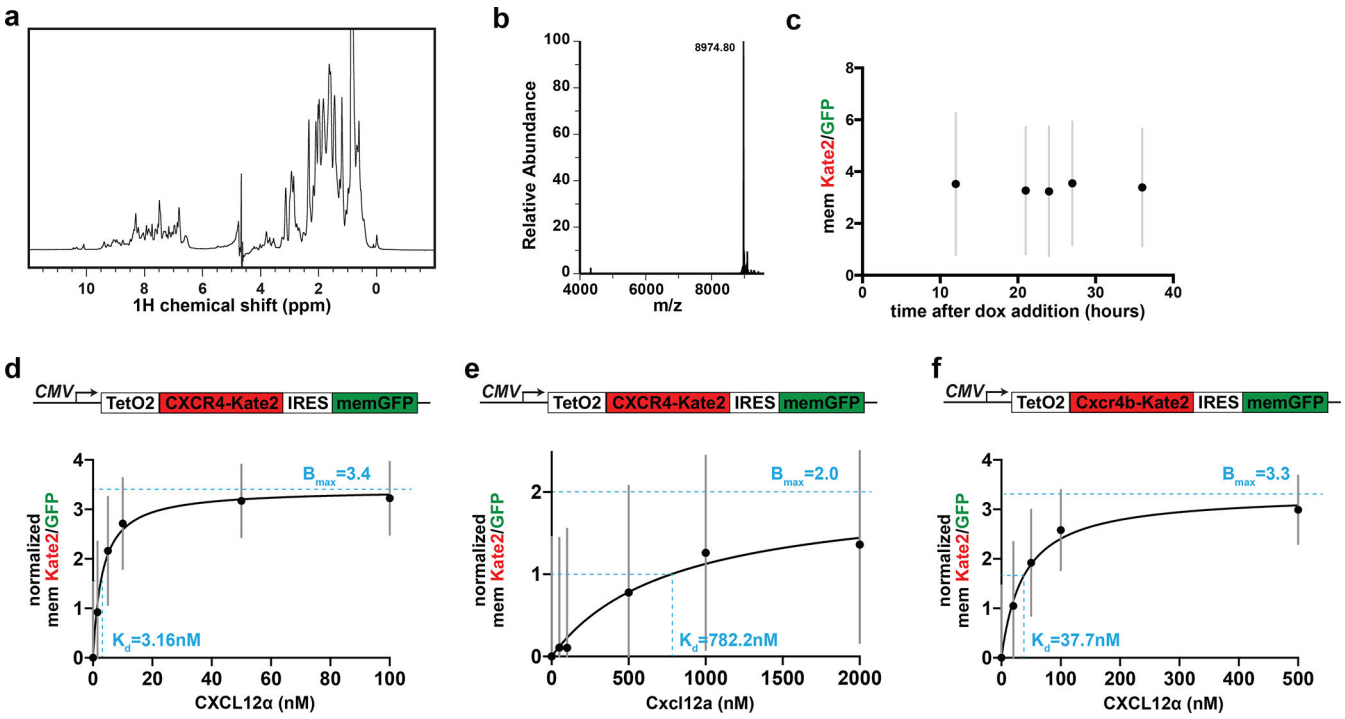

Extended Data Fig. 1. Measurements of the dissociation constants of Cxcl12 binding to Cxcr4.

a. One-dimensional 1H NMR of purified zebrafish Cxcl12a protein indicates protein folding since the amide region (6–10 ppm) of the spectrum contains peak dispersion, and upfield methyl peaks (peaks present at < 1 ppm) are present.

b. Mass spectrometry analysis of purified zebrafish Cxcl12a protein yielded an experimental weight of 8,974.8 daltons. This agrees with the expected weight of 8,975.6 daltons.

c. Ratio of membrane red-to-green fluorescence of the signaling sensor in T-REx 293 cells upon induction over time indicates stability of membrane red-to-green fluorescence ratios over time. Mean (dots) and SD (grey bars) are shown. n= 1240678, 1098868, 1076961, 3307144, 4260821 voxels analyzed for 12, 21, 24, 27, 36 hours post induction, respectively.

d. Human CXCL12α-human CXCR4 binding curve fitted to a one-site specific binding model. The mean (dots), SD (grey bars) and extracted K_d and B_{max} (dotted cyan lines) are indicated. n= 406108, 385060, 416200, 369700, 296400, 338460 voxels analyzed for 0, 1.5, 5, 10, 50, 100 nM concentrations, respectively.

e. Zebrafish Cxcl12a-human CXCR4 binding curve fitted to a one-site specific binding model. The mean (dots), SD (grey bars) and extracted K_d and B_{max} (dotted cyan lines) are

indicated. n= 248544, 308098, 350872, 324908, 282572, 259696 voxels analyzed for 0, 50, 100, 500, 1000, 2000 nM concentations, respectively.

f. Human CXCL12α -zebrafish Cxcr4b binding curve fitted to a one-site specific binding model. The mean (dots), SD (grey bars) and extracted K_d and B_{max} (dotted cyan lines) are indicated. n= 399632, 529120, 453188, 292848, 325436 voxels analyzed for 0, 20, 50, 100, 500 nM concentrations, respectively.

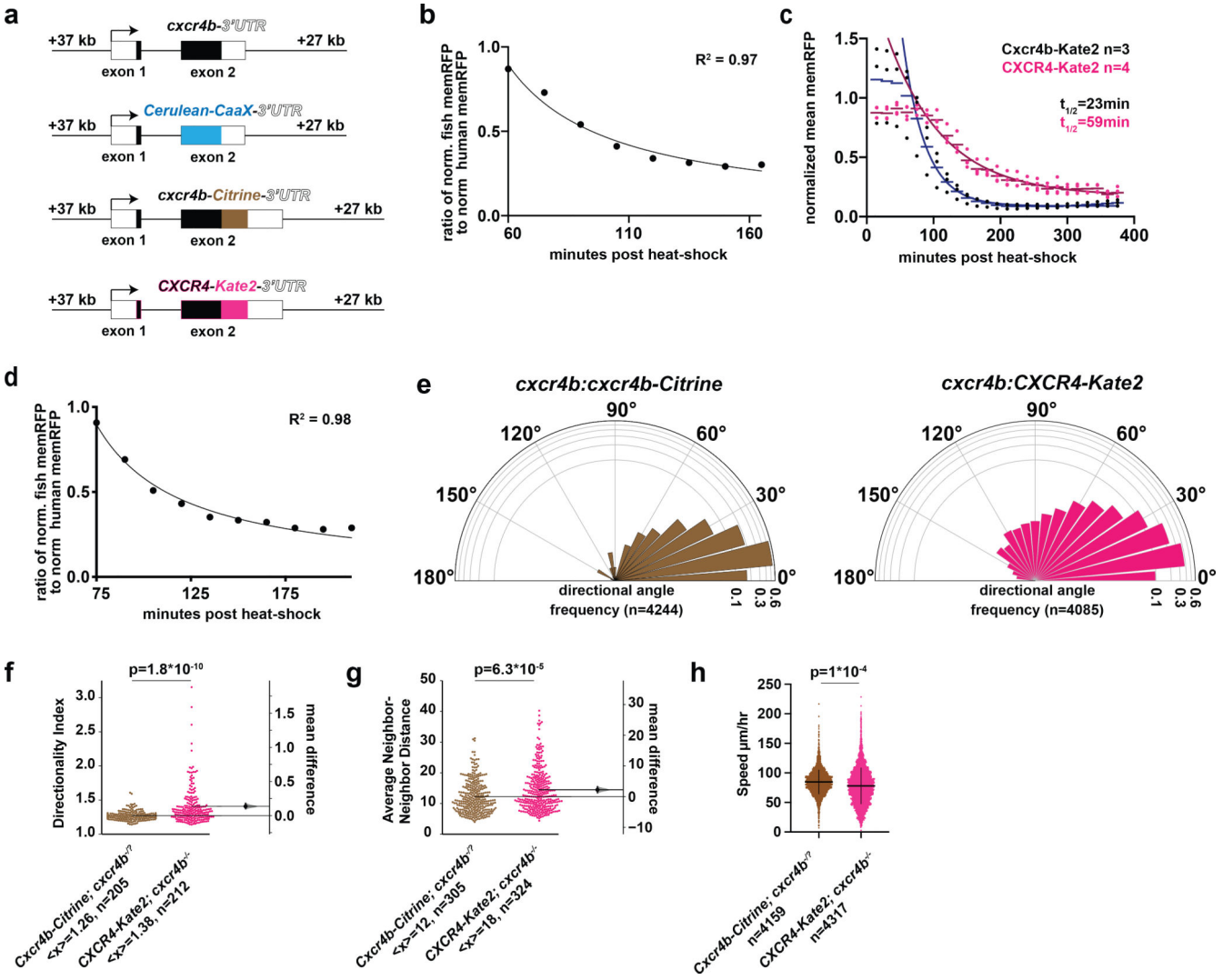

Extended Data Fig. 2. Low human Cxcr4 affinity to fish ligand affects cell migration.

a. Schematics of the *cxcr4b* BAC transgenes.

b. Ratio of normalized mean Cxcr4b-Kate2 fluorescence intensity to normalized mean CXCR4-Kate2 fluorescence intensity shown in Figure 2d fitted to the expected difference in receptor internalization for two receptors with K_ds of 3.4 nM and 782 nM (black line).

c. Membrane Cxcr4b-Kate2 and CXCR4-Kate2 fluorescence intensities with increasing levels of Cxcl12a normalized to heat-shocked control embryos over time. Individual means (circles), averaged means (horizontal lines), and fit of the data (t > 60 min) to a one-exponential decay model (lines) are indicated for Cxcr4b-Kate2 (black, n=3 embryos) and

CXCR4-Kate2 (magenta, n=4 embryos). Scale bar is 20 μm. Note, this is a biologically independent experiment of Figure 2d.

d. Ratio of normalized mean Cxcr4b-Kate2 fluorescence intensity to normalized mean CXCR4-Kate2 fluorescence intensity shown in c fitted to the expected difference in receptor internalization for two receptors with K_ds of 3.4 nM and 782 nM (black line).

e. Semi-circular histogram plots of the directional angle frequencies of leader cells in *cxcr4b:cxcr4b-Citrine*; *cxcr4b*$^{-/-}$ or *cxcr4b*$^{-/+}$ (left, n=4244) and *cxcr4b:CXCR4-Kate2*; *cxcr4b*$^{-/-}$ primordia (right, n=4085) from H2A-GFP labeled nuclei (Video 4). Radial axes are $\log_{10}$-scale. The difference in directional angle distributions is significantly different (p = 0.0001, two-sided Kolmogorov-Smirnov test).

f. Directional indices of leader cells in *cxcr4b:cxcr4b-Citrine*; *cxcr4b*$^{-/-}$ or *cxcr4b:cxcr4b-Citrine*; *cxcr4b*$^{-/+}$ (n=205) and *cxcr4b:CXCR4-Kate2*; *cxcr4b*$^{-/-}$ primordia (n=212) (Video 4). p = 1.8×10^{-10}, two-sided Mann-Whitney test.

g. Neighbor-neighbor distances for leader cells in *cxcr4b:cxcr4b-Citrine*; *cxcr4b*$^{-/-}$ or *cxcr4b*$^{-/+}$ (n=305) and *cxcr4b:CXCR4-Kate2*; *cxcr4b*$^{-/-}$ primordia (n=324) (Video 4). p = 6.3×10^{-5}, two-sided Mann-Whitney test.

In f and g, the mean difference is shown as a Gardner-Altman estimation plot. Both groups are plotted on the left axes; the mean difference is plotted on the right axes as a bootstrap sampling distribution. Mean (horizontal line), mean difference (dot), the 95% confidence interval (vertical bars) are indicated.

h. Speed of leader cells in *cxcr4b:cxcr4b-Citrine*; *cxcr4b*$^{-/-}$ or *cxcr4b*$^{-/+}$ (n=4159) and *cxcr4b:CXCR4-Kate2*; *cxcr4b*$^{-/-}$ primordia (n=4317, Video 4). Mean (horizontal line) and SD (vertical bars) are indicated. The difference in speed is significantly different, p = 0.0001, two-sided Kolmogorov-Smirnov test.

In c, e-h, n represents the number of tracked cells extracted from seven embryos for each genetic scenario.

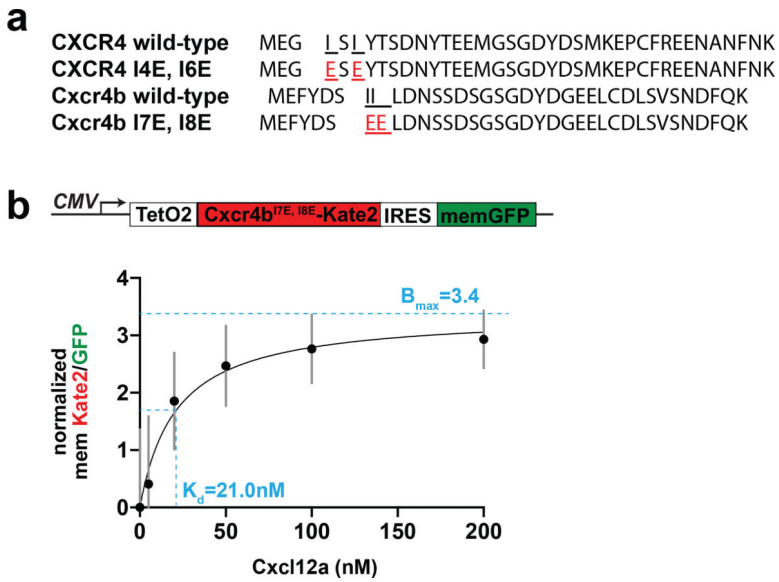

Extended Data Fig. 3. Determination of the binding affinity of Cxcl12a for Cxcr4b^{I7E,I8E}.

a. Comparison of the N-terminal extracellular sequence of human and zebrafish Cxcr4. Mutations known to lower the affinity to Cxcl12 are highlighted in red for the human CXCR4 and, based on sequence conservation, for the zebrafish Cxcr4b receptors.
b. Top. Construct of the Cxcl12a-signaling sensor for the Cxcr4b^{I7E,I8E} receptor expressed in T-REx 293 cells. Bottom. Zebrafish Cxcl12a- zebrafish Cxcr4b^{I7E,I8E} binding curve fitted to a one-site specific binding model. The mean (dots), SD (grey bars) and extracted K_d and B_{max} (dotted cyan lines) are indicated. n=410452, 581584, 386060, 266532, 300640, 203284 voxels analyzed for 0, 5, 20, 50, 100, 200 nM concentrations, respectively.

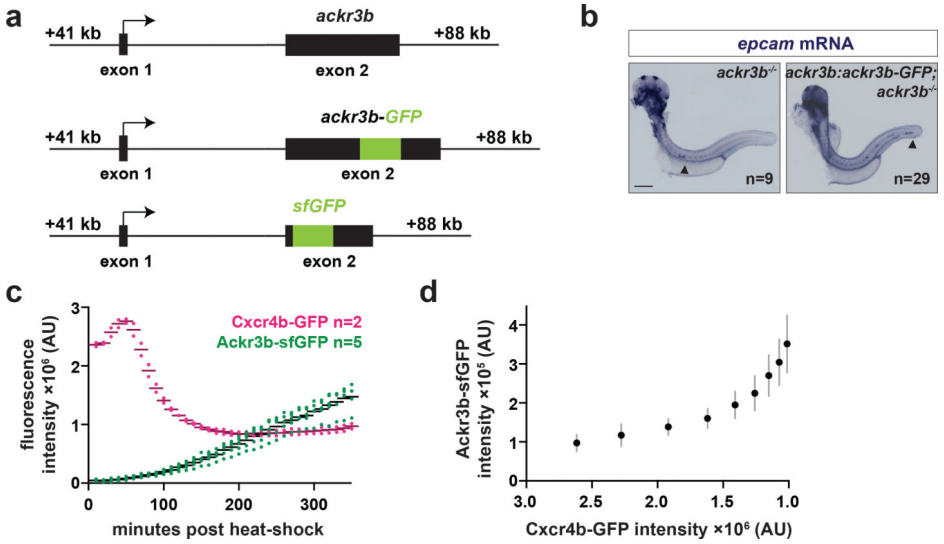

Extended Data Fig. 4. Ackr3b BAC transgenes recapitulate Acrk3b function.

a. Schematics of the *ackr3b* BAC transgenes. Exons 1 and 2 of *ackr3b* and upstream and downstream genomic regions are indicated. The unmodified genomic locus is shown for reference (top). For the *ackr3b:ackr3b-GFP* transgene, GFP is inserted before the stop codon in exon 2 (middle). For the *ackr3b* transcriptional reporter, the coding sequence of *ackr3b* in exon 2 was replaced with the coding sequence for *sfGFP* (bottom).
b. Analysis of completed primordium migration in *ackr3b*−/− (n=9 embryos) and *ackr3b*−/−; *ackr3b:ackr3b-GFP* embryos (n=29 embryos) using *in situ* hybridization against the primordium marker *epcam* at 48 hpf. The arrowhead indicates the position of the primordium. Scale bar corresponds to 200 μm.
c. Total Cxcr4b-GFP (n=2 embryos) and Ackr3b-sfGFP (n=5 embryos) fluorescence intensities within the primordia with increasing levels of Cxcl12a over time. Note that decreasing Cxcr4b-GFP intensity reflects increasing Cxcl12a levels outside the primordium. Fluorescence intensities in primordia of individual embryos (circles) and averaged total fluorescence intensities (horizontal lines) are indicated. The initial rate of Cxcr4b-GFP intensity decrease is 2.8×10^{-2} AU/s and initial rate of Ackr3b-GFP intensity increase is 1.8×10^{-3} AU/s. The experiment was independently repeated once with similar results.
d. Increasing Ackr3b-sfGFP expression plotted against decreasing Cxcr4b-GFP expression from 50 min to 200 min after induction of increasing Cxcl12a expression as shown in c. The initial rate of Ackr3b-sfGFP intensity increase per Cxcr4b-GFP intensity decrease is 16.

Mean (dot) and SD (grey bars) are indicated. n as indicated in c represents the number of embryos.

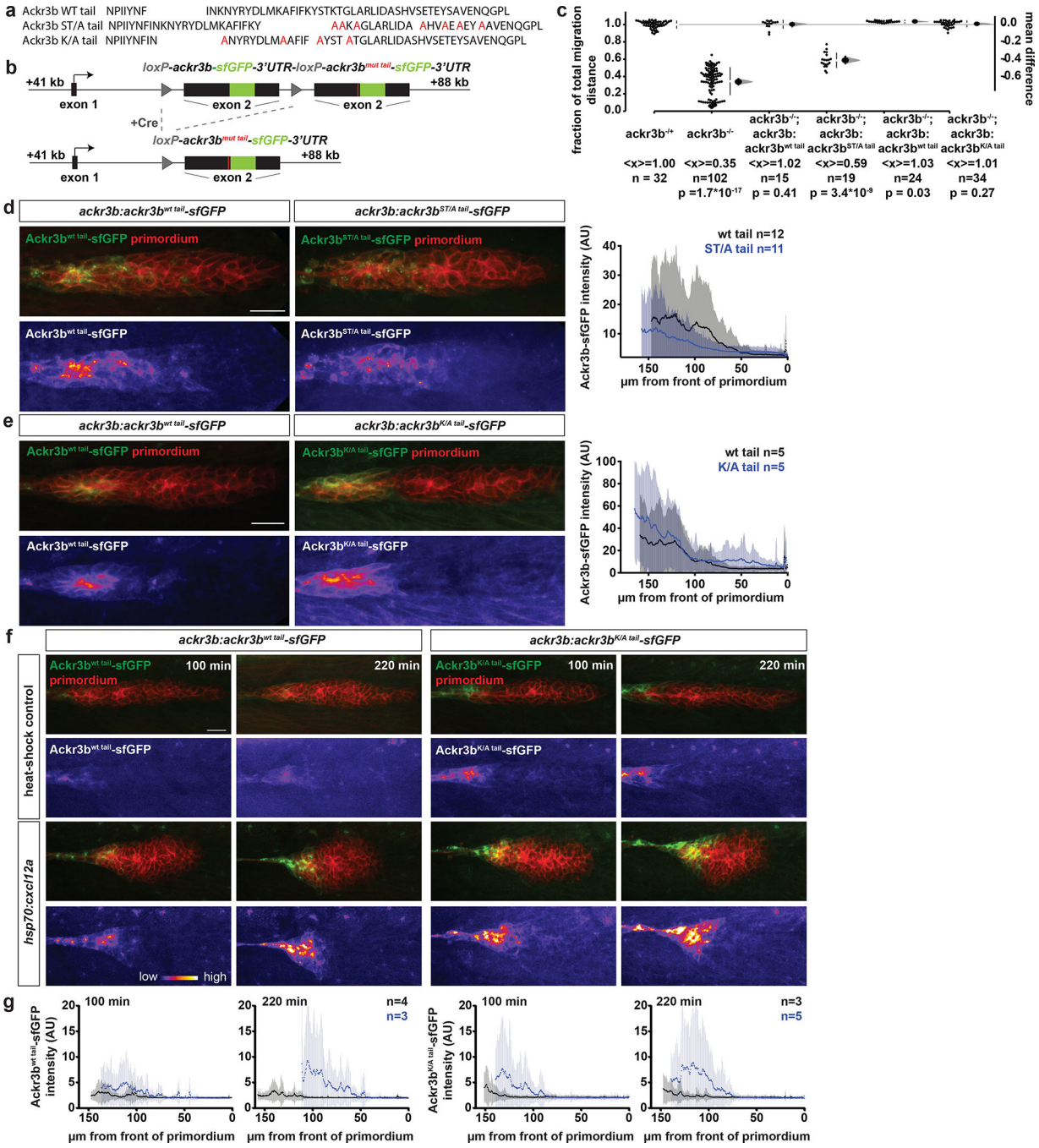

Extended Data Fig. 5. Characterization of Ackr3b ST/A and K/A cytoplasmic tail mutants.

a. Amino acid sequence of the cytoplasmic tail of wild-type, ST/A and K/A mutant Ackr3b (in red).

b. Design of *ackr3b-sfGFP* control and cytoplasmic tail mutant BAC transgenic lines.

c. Quantification of migration distance of primordia in 48 hpf embryos of indicated genotypes. The mean difference for five comparisons against the shared *ackr3b*$^{-/+}$ control embryos are shown as a Cumming estimation plot. The raw data is plotted on the left axis. On the right axis, the mean differences are plotted as bootstrap sampling distributions. Mean differences (dots) and 95% confidence interval (vertical bars) are indicated for *ackr3b*$^{-/+}$ (<x>=1.00, n=32), *ackr3b*$^{-/-}$ (<x>=0.35, n=102, p=1.7×10^{-17}), *ackr3b*$^{-/-}$*; ackr3b:ackr3b*$^{wt\ tail}$*-sfGFP* (<x>=1.02, n=15, p=0.41), *ackr3b*$^{-/-}$*; ackr3b:ackr3b*$^{ST/A\ tail}$*-sfGFP* (<x>=0.59, n=19, p=3.4×10^{-9}), *ackr3b*$^{-/-}$*; ackr3b:ackr3b*$^{wt\ tail}$*-sfGFP* (<x>=1.03, n=24, p=0.03), and *ackr3b*$^{-/-}$*; ackr3b:ackr3b*$^{K/A\ tail}$*-sfGFP* (<x>=1.01, n=34, p=0.27), where <x> represents the mean, n represents the number of embryos, and p represents p-values (two-sided Mann-Whitney test).

d and e. Left. Ackr3b$^{wt\ tail}$-sfGFP and Ackr3b$^{ST/A\ tail}$-sfGFP (in d), and Ackr3b$^{wt\ tail}$-sfGFP and Ackr3b$^{K/A\ tail}$-sfGFP (in e) fluorescence intensities in the primordia are shown together with the primordium marker *prim:lyn$_2$mCherry* (top panels) and separately as a heat-map (bottom panels). The fluorescence intensities in all images are scaled identically. Right. Mean (dots) and SD (vertical bars) of Ackr3b-sfGFP fluorescence intensities along the front-back axis of primordia in wild-type and ST/A tail embryos (in d) and wild-type and K/A tail embryos (in e). n=12 and 11 embryos for wt and ST/A tail, respectively and n=5 embryos for wt and K/A tail.

f. Response of Ackr3b$^{wt\ tail}$-sfGFP and Ackr3b$^{K/A\ tail}$-sfGFP fusion proteins in the primordium of embryos with increasing Cxcl12a levels. The control *ackr3b:loxP-ackr3b*$^{wt\ tail}$*-sfGFP-stop-loxP-ackr3b*$^{K/A\ tail}$*-sfGFP; ackr3b*$^{-/-}$*; prim:lyn$_2$mCherry* and the experimental *ackr3b:ackr3b*$^{K/A\ tail}$*-sfGFP; ackr3b*$^{-/-}$*; prim:lyn$_2$mCherry; hsp70:cxcl12a* embryos were imaged at indicated times past a 30 min heat-shock that induced Cxcl12a expression from the heat shock promoter. The Ackr3b-sfGFP fluorescence intensities in the primordia are shown together with the primordium marker *prim:lyn$_2$mCherry* (top panels) and separately as a heat-map (bottom panels). The fluorescence intensities in all images are scaled identically and quantified in g.

g. Mean Ackr3b$^{wt\ tail}$-sfGFP and Ackr3b$^{K/A\ tail}$-sfGFP fluorescence intensities (dots) and SD (vertical bars) of heat-shocked control embryos (black, n=4 and 3 embryos, respectively) and Cxcl12a-overexpressing embryos (blue, n=3 and 5 embryos, respectively) along the front-back axis of primordia.

In d, e, and f, the scale bar corresponds to 20 μm. Anterior is to the left and the front of the primordium is to the right.

Supplementary Material

Refer to Web version on PubMed Central for supplementary material.

Acknowledgement

We thank T. Colak-Champollion, N. Yamaguchi, D. Nagelberg, J. Torres-Vazquez and his lab, R. Lehmann, C. Desplan, A. Mogilner and T. Prüstel for critical discussions, L. Lan for help with Matlab scripts, T. Gerson and J. Proietti for excellent fish care, and F. Fuentes, J. Ryou, and A. Epifano for help with cloning. This work was supported by American Heart Association fellowship (18PRE33960083 to S.L.) and NIH (R01NS102322 to H.K., F30HD079229 to J.W. and R01 AI058072 to B.F.V.) and, in part, by the intramural program of NIH/NIAID (M.M-S.)

References

1. Ueda M & Shibata T Stochastic Signal Processing and Transduction in Chemotactic Response of Eukaryotic Cells. Biophys. J 93, 11–20 (2007). [PubMed: 17416630]
2. Schwarz J et al. Dendritic Cells Interpret Haptotactic Chemokine Gradients in a Manner Governed by Signal-to-Noise Ratio and Dependent on GRK6. Curr Biol 27, 1314–1325 (2017). [PubMed: 28457871]
3. Rappel W-J & Levine H Receptor noise limitations on chemotactic sensing. Proc Natl Acad Sci USA 105, 19270–19275 (2008). [PubMed: 19064934]
4. Fuller D et al. External and internal constraints on eukaryotic chemotaxis. Proc Natl Acad Sci USA 107, 9656–9659 (2010). [PubMed: 20457897]
5. Herzmark P et al. Bound attractant at the leading vs. the trailing edge determines chemotactic prowess. Proc Natl Acad Sci USA 104, 13349–13354 (2007). [PubMed: 17684096]
6. Van Haastert PJM & Postma M Biased Random Walk by Stochastic Fluctuations of Chemoattractant-Receptor Interactions at the Lower Limit of Detection. Biophys. J 93, 1787–1796 (2007). [PubMed: 17513372]
7. David NB et al. Molecular basis of cell migration in the fish lateral line: role of the chemokine receptor CXCR4 and of its ligand, SDF1. Proc Natl Acad Sci USA 99, 16297–16302 (2002). [PubMed: 12444253]
8. Donà E et al. Directional tissue migration through a self-generated chemokine gradient. Nature 503, 285–289 (2013). [PubMed: 24067609]
9. Venkiteswaran G et al. Generation and Dynamics of an Endogenous, Self-Generated Signaling Gradient across a Migrating Tissue. Cell 155, 674–687 (2013). [PubMed: 24119842]
10. Hanes MS et al. Dual Targeting of the Chemokine Receptors CXCR4 and ACKR3 with Novel Engineered Chemokines. J Biol Chem 290, 22385–22397 (2015). [PubMed: 26216880]
11. Burns JM et al. A novel chemokine receptor for SDF-1 and I-TAC involved in cell survival, cell adhesion, and tumor development. J Exp Med 203, 2201–2213 (2006). [PubMed: 16940167]
12. Ziarek JJ et al. Structural basis for chemokine recognition by a G protein-coupled receptor and implications for receptor activation. Science Signaling 10, (2017).
13. Boldajipour B et al. Control of Chemokine-Guided Cell Migration by Ligand Sequestration. Cell 132, 463–473 (2008). [PubMed: 18267076]
14. Sánchez-Alcañiz JA et al. Cxcr7 controls neuronal migration by regulating chemokine responsiveness. Neuron 69, 77–90 (2011). [PubMed: 21220100]
15. Kennedy JE & Marchese A Regulation of GPCR Trafficking by Ubiquitin Trafficking of GPCRs 132, 15–38 (Elsevier Inc., 2015).
16. Moore CAC, Milano SK & Benovic JL Regulation of receptor trafficking by GRKs and arrestins. Annu. Rev. Physiol 69, 451–482 (2007). [PubMed: 17037978]
17. Hoffmann F et al. Rapid uptake and degradation of CXCL12 depend on CXCR7 carboxyl-terminal serine/threonine residues. Journal of Biological Chemistry 287, 28362–28377 (2012).
18. Canals M et al. Ubiquitination of CXCR7 controls receptor trafficking. PLoS ONE 7, e34192 (2012). [PubMed: 22457824]
19. Saaber F et al. ACKR3 Regulation of Neuronal Migration Requires ACKR3 Phosphorylation, but Not β-Arrestin. CellReports 26, 1473–1488.e9 (2019).
20. Swaney KF, Huang C-H & Devreotes PN Eukaryotic Chemotaxis: A Network of Signaling Pathways Controls Motility, Directional Sensing, and Polarity. Annu. Rev. Biophys 39, 265–289 (2010). [PubMed: 20192768]
21. Mantovani A, Bonecchi R & Locati M Tuning inflammation and immunity by chemokine sequestration: decoys and more. Nat Rev Immunol 6, 907–918 (2006). [PubMed: 17124512]
22. Korsensky L & Ron D Regulation of FGF signaling: Recent insights from studying positive and negative modulators. Semin Cell Dev Biol 53, 1–14 (2016). [PubMed: 27206955]
23. Chung AS & Ferrara N Developmental and Pathological Angiogenesis. Annu. Rev. Cell Dev. Biol. 27, 563–584 (2011). [PubMed: 21756109]

24. Pocha SM & Montell DJ Cellular and Molecular Mechanisms of Single and Collective Cell Migrations in Drosophila: Themes and Variations. Annu. Rev. Genet. 48, 295–318 (2014). [PubMed: 25421599]
25. Friedl P & Gilmour D Collective cell migration in morphogenesis, regeneration and cancer. Nat Rev Mol Cell Biol 10, 445–457 (2009). [PubMed: 19546857]
26. Knaut H, Werz C, Geisler R, Nüsslein-Volhard C & Tübingen 2000 Screen Consortium. A zebrafish homologue of the chemokine receptor Cxcr4 is a germ-cell guidance receptor. Nature 421, 279–282 (2003). [PubMed: 12508118]
27. Bussmann J, Wolfe SA & Siekmann AF Arterial-venous network formation during brain vascularization involves hemodynamic regulation of chemokine signaling. Development 138, 1717–1726 (2011). [PubMed: 21429983]
28. Valentin G, Haas P & Gilmour D The chemokine SDF1a coordinates tissue migration through the spatially restricted activation of Cxcr7 and Cxcr4b. Curr Biol 17, 1026–1031 (2007). [PubMed: 17570670]
29. Kettleborough RNW et al. A systematic genome-wide analysis of zebrafish protein-coding gene function. Nature 496, 494–497 (2013). [PubMed: 23594742]
30. Knaut H, Blader P, Strähle U & Schier AF Assembly of trigeminal sensory ganglia by chemokine signaling. Neuron 47, 653–666 (2005). [PubMed: 16129396]
31. Haas P & Gilmour D Chemokine signaling mediates self-organizing tissue migration in the zebrafish lateral line. Dev Cell 10, 673–680 (2006). [PubMed: 16678780]
32. Wang J et al. Anosmin1 Shuttles Fgf to Facilitate Its Diffusion, Increase Its Local Concentration, and Induce Sensory Organs. Dev Cell 46, 751–766.e12 (2018). [PubMed: 30122631]
33. Kozlovskaja-Gumbrienė A et al. Proliferation-independent regulation of organ size by Fgf/Notch signaling. eLife 6, (2017).
34. Fuentes F, Reynolds E, Lewellis SW, Venkiteswaran G & Knaut H A Plasmid Set for Efficient Bacterial Artificial Chromosome (BAC) Transgenesis in Zebrafish. G3: Genes|Genomes|Genetics (2016). doi:10.1534/g3.115.026344
35. Yamaguchi N, colak-Champollion T & Knaut H zGrad is a nanobody-based degron system that inactivates proteins in zebrafish. eLife 8, 4640 (2019).
36. colak-Champollion T et al. Cadherin-Mediated Cell Coupling Coordinates Chemokine Sensing across Collectively Migrating Cells. Curr Biol 29, 2570–2579.e7 (2019). [PubMed: 31386838]
37. Tsai W-H Moment-preserving thresolding: A new approach. Computer Vision, Graphics, and Image Processing 29, 377–393 (1985).
38. Lauffenburger DA & Linderman JJ Receptors: models for binding, trafficking, and signaling. 1993 New York: Oxford University Press
39. Thisse C & Thisse B High-resolution in situ hybridization to whole-mount zebrafish embryos. Nature Protocols 3, 59–69 (2008). [PubMed: 18193022]
40. Ho J, Tumkaya T, Aryal S, Choi H & Claridge-Chang A Moving beyond P values: data analysis with estimation graphics. Nat Meth 16, 1–4 (2019).

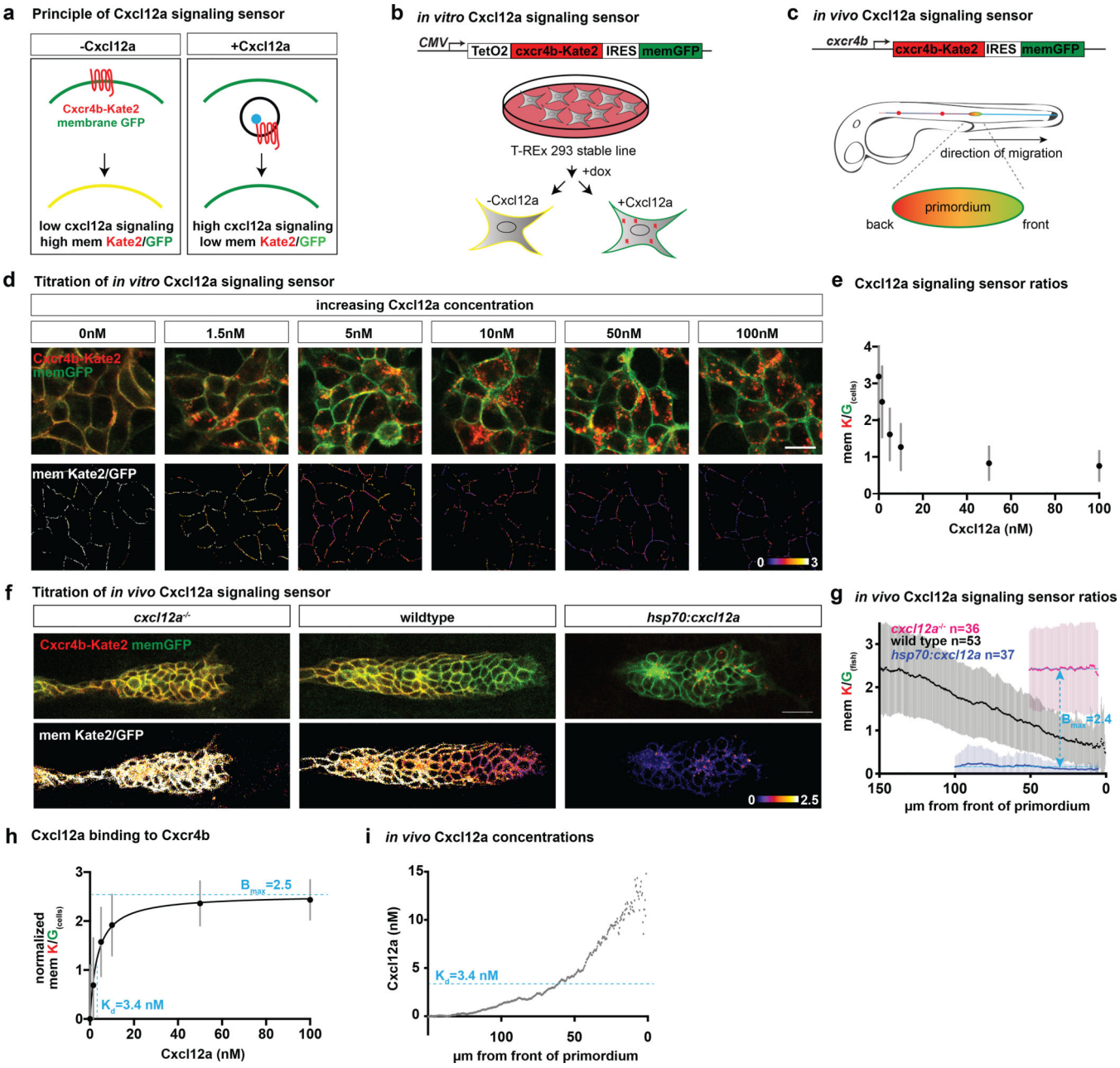

Figure 1. The Cxcl12a concentrations are centered around the K_d of Cxcl12a for Cxcr4b during primordium migration.

a. Principle of the Cxcl12a-signaling sensor.

b. Construct and schematic of Cxcl12a-signaling sensor in cultured cells.

c. Construct and schematic of Cxcl12a-signaling sensor in zebrafish.

d. Top. Response of the Cxcl12a-signaling sensor in T-REx 293 cells to different Cxcl12a concentrations. Bottom. Corresponding membrane red-to-green fluorescence intensity ratio images pseudo-colored as heat maps. Scale bar is 20 μm and the heat maps range from 0 to 3.

e. Quantification of the membrane red-to-green fluorescence ratio of the signaling sensor in T-REx 293 cells exposed to indicated Cxcl12a concentrations. Mean (dots) and SD (grey bars) are indicated. n=251928, 269836, 280004, 266520, 245324, 186988 voxels analyzed for 0, 1.5, 5, 10, 50, 100 nM concentrations, respectively.

f. Top. Single confocal sections of primordia expressing the Cxcl12a-signaling sensor in embryos with different Cxcl12a levels at 36 hpf. Bottom. Corresponding images of the membrane red-to-green fluorescence intensity ratios pseudo-colored as heat maps. Scale bar is 20 μm and the heat maps range from 0 to 2.5. Anterior is to the left and the direction of primordium migration is to the right.

g. Quantification of the membrane red-to-green fluorescence intensity ratios of the Cxcl12-signaling sensor in embryos with different Cxcl12a levels. Mean (dots) and SD (vertical bars) are indicated for *cxcl12a*$^{-/-}$ (magenta, n=36 embryos), wild-type and *cxcl12a*$^{-/+}$ (black, n=53 embryos), and *cxcl12a*-overexpressing embryos (blue, n=37 embryos). Averaged means across the front-to-back primordium axis for *cxcl12a*$^{-/-}$ and *cxcl12a*-overexpressing embryos are indicated as dotted horizontal lines (cyan). The front of the primordium corresponds to 0 μm on the x-axis. The maximal change of the membrane red-to-green fluorescence intensity ratio in embryos lacking and over-expressing Cxcl12a is indicated as B_{max}.

h. Cxcl12a-Cxcr4b binding curve of the normalized Cxcl12a signaling sensor ratios from cell culture in e fitted to a one-site specific binding model (black line) to extract the K_d and B_{max} (dotted cyan lines). Mean (dots) and SD (grey bars) are indicated.

i. Plot of Cxcl12a concentrations across the front-back axis of the primordium. The Cxcl12a-Cxcr4b K_d is indicated as a dotted cyan line.

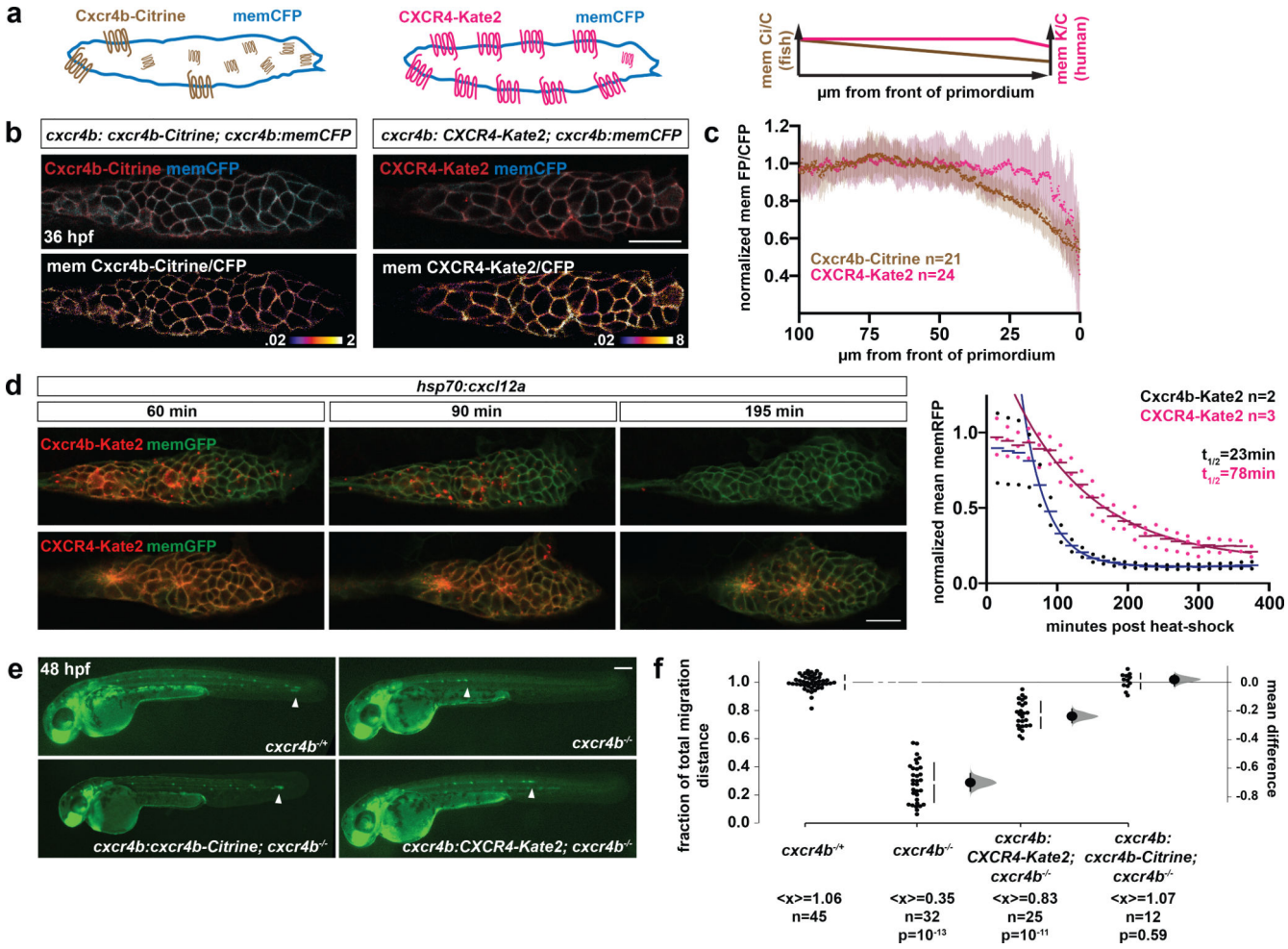

Figure 2. Human CXCR4 cannot support directional primordium migration.

a. Schematic and hypothesis of replacing the zebrafish Cxcr4b with human CXCR4.

b. Top. Single confocal section of 36 hpf primordia expressing membrane-bound CFP and zebrafish Cxcr4b-Citrine or human CXCR4-Kate2. Bottom. Corresponding images of the membrane ratio of Cxcr4b-Citrine and CXCR4-Kate2 to CFP pseudo-colored as heat maps. Scale bar is 20 µm.

c. Quantification of receptor internalization shown as the ratio of membrane Cxcr4b-Citrine or CXCR4-Kate2 fluorescence to membrane CFP fluorescence normalized to the average fluorescence ratios in the primordium's back. Mean (dots) and SD (vertical bars) are indicated for Cxcr4b-Citrine (orange, n=21 embryos) and CXCR4-Kate2 (magenta, n=24 embryos).

d. Left. Single confocal sections of primordia in *cxcr4b:cxcr4b-Kate2*; *cldnB:lyn$_2$GFP*; *hsp70:cxcl12a* (top) and *cxcr4b:CXCR4-Kate2*; *cldnB:lyn$_2$GFP*; *hsp70:cxcl12a* embryos (bottom) at indicated times past the end of a 10 min heat shock that induced the over-expression of Cxcl12a. Right. Membrane Cxcr4b-Kate2 and CXCR4-Kate2 fluorescence intensities with increasing levels of Cxcl12a normalized to heat-shocked control embryos over time (Video 1). Individual means (circles), averaged means (horizontal lines), and fit of the data (t > 60 min) to a one-exponential decay model (lines) are indicated for Cxcr4b-

Kate2 (black, n=2 embryos) and CXCR4-Kate2 (magenta, n=3 embryos). Scale bar is 20 μm.

e. Images of *cldnB:lyn$_2$GFP* embryos of indicated genotypes at 48 hpf. Arrowheads indicate the position of the primordium. Scale bar corresponds to 200 μm.

f. Quantification of the migration distance shown in e. The mean difference for three comparisons against the shared *cxcr4b*$^{-/+}$ control embryos are shown as a Cumming estimation plot. The raw data is plotted on the left axis. On the right axis, mean differences are plotted as bootstrap sampling distributions. Mean differences (dots) and 95% confidence interval (vertical bars) are indicated for *cxcr4b*$^{-/+}$ (<x>=1.06, n=45), *cxcr4b*$^{-/-}$ (<x>=0.35, n=32, p=10^{-13}), *cxcr4b:CXCR4-Kate2; cxcr4b*$^{-/-}$ (<x>=0.83, n=25, p=10^{-11}), and *cxcr4b:cxcr4b-Citrine; cxcr4b*$^{-/-}$ (<x>=1.07, n=12, p=0.59), where <x> represents the mean, n represents the number of embryos, and p represents p-values (two-sided Mann-Whitney test).

In all images, anterior is to the left and primordium front is to the right.

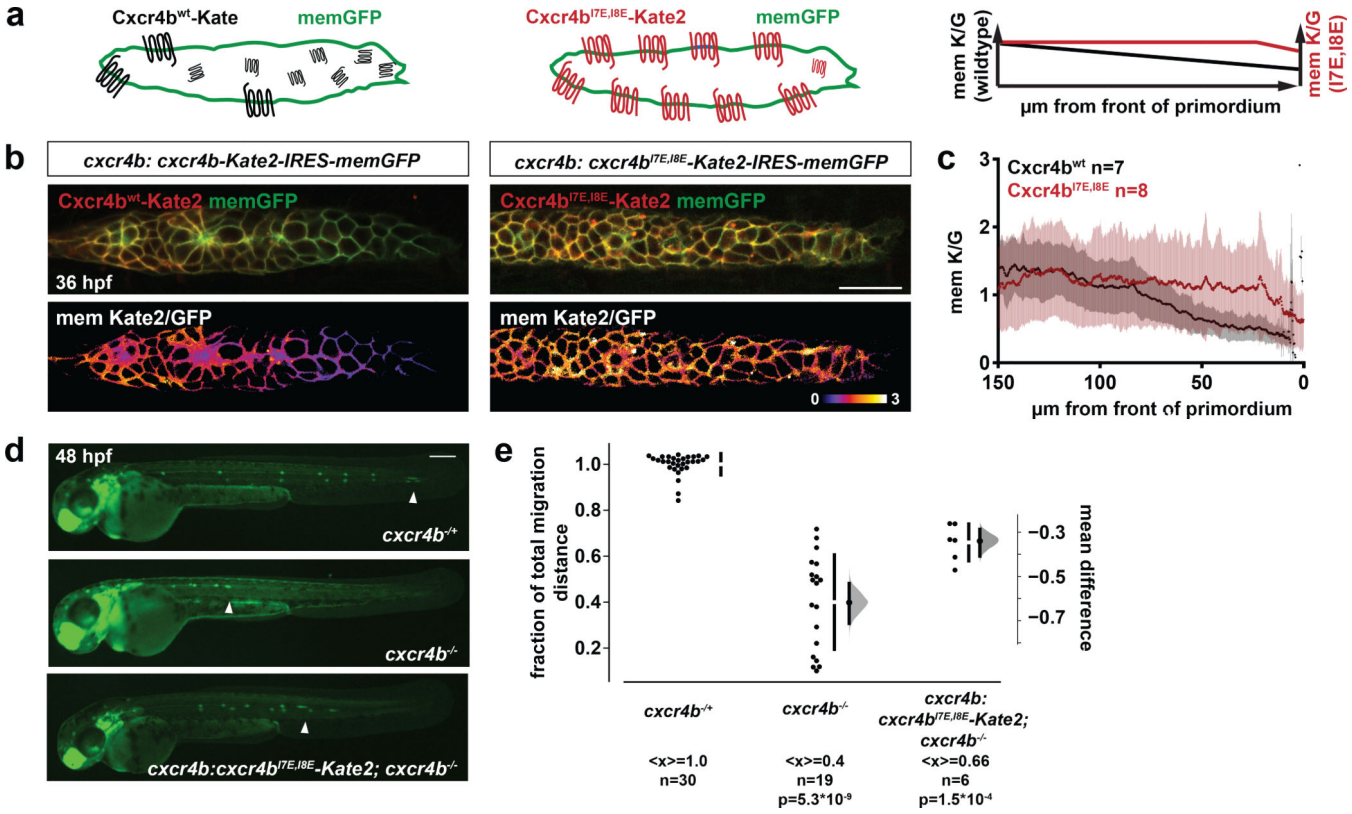

Figure 3. Lowering the affinity of Cxcr4b for Cxcl12a impairs directional migration.

a. Schematic and hypothesis of lowering zebrafish Cxcr4b's affinity for Cxcl12a.

b. Top. Single confocal sections of primordia expressing membrane-bound GFP and zebrafish Cxcr4b^{wt}-Kate2 (left) or Cxcr4b^{I7E,I8E}-Kate2 (right) at 36 hpf. Bottom. Corresponding images of the membrane ratio of Cxcr4b^{wt}-Kate2 and Cxcr4b^{I7E,I8E}-Kate2 to GFP pseudo-colored as heat maps. Scale bar is 20 µm. Anterior is to the left and the front of the primordium is to the right.

c. Quantification of Cxcr4b^{wt} and Cxcr4b^{I7E,I8E} internalization shown as the ratio of membrane Kate2 fluorescence to membrane GFP fluorescence. Mean fluorescence intensity ratios (dots) and SD (vertical bars) are indicated for Cxcr4b^{wt}-Kate2 (black, n=7 embryos) Cxcr4b^{I7E,I8E}-Kate2 (red, n=8 embryos).

d. Images of *cldnB:lyn$_2$GFP* embryos of indicated genotypes at 48 hpf. Arrowheads indicate the position of the primordium. Scale bar corresponds to 200 µm.

e. Quantification of the migration distance of primordia in 48 hpf embryos of indicated genotypes shown in d. The mean difference for two comparisons against the shared *cxcr4b* $^{-/+}$ control embryos are shown as a Cumming estimation plot. The raw data is plotted on the left axis. On the right axis, the mean differences are plotted as bootstrap sampling distributions. Mean differences (dots) and 95% confidence interval (vertical bars) are indicated for *cxcr4b*$^{-/+}$ (<x>=1.0, n=30), *cxcr4b*$^{-/-}$ (<x>=0.4, n=19, p=5.3×10^{-9}), and *cxcr4b:cxcr4b*$^{I7E,\ I8E}$*-Kate2*; *cxcr4b*$^{-/-}$ (<x>=0.66, n=6, p=1.5×10^{-4}), where <x> represents the mean, n represents the number of embryos, and p represents p-values (two-sided Mann-Whitney test).

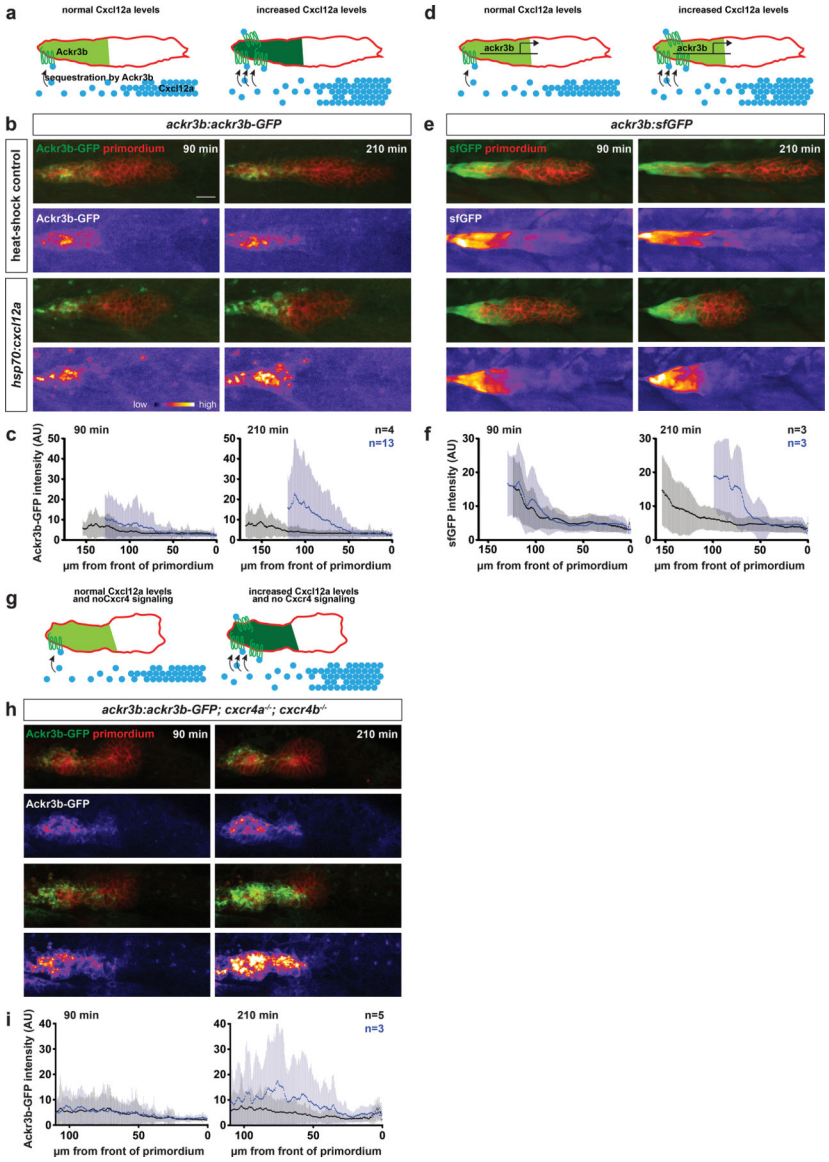

Figure 4. Ackr3b feeds back on increased Cxcl12a levels.

a. Schematic and hypothesis of Cxcl12a upregulation on the levels of Ackr3b protein in wild-type embryos.

b. Expression of Ackr3b-GFP in the primordium of control *ackr3b:ackr3b-GFP*; *prim:lyn$_2$mCherry* embryos and Cxcl12a-upregulating *ackr3b:ackr3b-GFP*; *prim:lyn$_2$mCherry*; *hsp70:cxcl12a* embryos at indicated times past a 30 min heat shock.

c. Mean Ackr3b-GFP fluorescence intensities (dots) and SD (vertical bars) along the front-back axis of primordia in heat-shock control (black, n=4 embryos) and Cxcl12a-over-expressing wild-type embryos (blue, n=13 embryos) shown in b.

d. Schematic and hypothesis of Cxcl12a upregulation on the levels of *ackr3b* transcription in wild-type embryos.

e. Expression of the *ackr3b* transcriptional reporter in the primordium of control *ackr3b:sfGFP*; *prim:lyn$_2$mCherry* embryos and Cxcl12a-upregulating *ackr3b:sfGFP*; *prim:lyn$_2$mCherry*; *hsp70:cxcl12a* embryos at indicated times past a 30 min heat shock.
f. Mean sfGFP fluorescence intensities (dots) and SD (vertical bars) along the front-back axis of primordia in heat-shock control (black, n=3 embryos) and Cxcl12a-over-expressing *ackr3b:sfGFP* (blue, n=3 embryos) embryos shown in e.
g. Schematic and hypothesis of Cxcl12a upregulation on the levels of Ackr3b protein in *cxcr4* mutant embryos.
h. Expression of Ackr3b-GFP in the primordium of Cxcr4-deficient control *ackr3b:ackr3b-GFP*; *prim:lyn$_2$mCherry*; *cxcr4a*$^{-/-}$; *cxcr4b*$^{-/-}$ embryos and Cxcl12a-upregulating *ackr3b:ackr3b-GFP*; *prim:lyn$_2$mCherry*; *hsp70:cxcl12a*; *cxcr4a*$^{-/-}$; *cxcr4b*$^{-/-}$ embryos at indicated times past a 30 min heat shock.
i. Mean Ackr3b-GFP fluorescence intensities (dots) and SD (vertical bars) along the front-back axis of primordia in heat-shock control (black, n=5 embryos) and Cxcl12a-over-expressing (blue, n=3 embryos) *cxcr4a*; *cxcr4b* mutant embryos shown in h.
In b, e, and h, the Ackr3b-GFP and sfGFP fluorescence intensities in the primordia are shown together with the primordium marker *prim:lyn$_2$mCherry* (top panels) and separately as a heat-map (bottom panels). The fluorescence intensities in each column of images are scaled identically. Scale bar corresponds to 20 μm. Anterior is to the left and the front of the primordium is to the right. Note that the embryos were wild-type for *ackr3b*. 0 μm represents the front of the primordium.

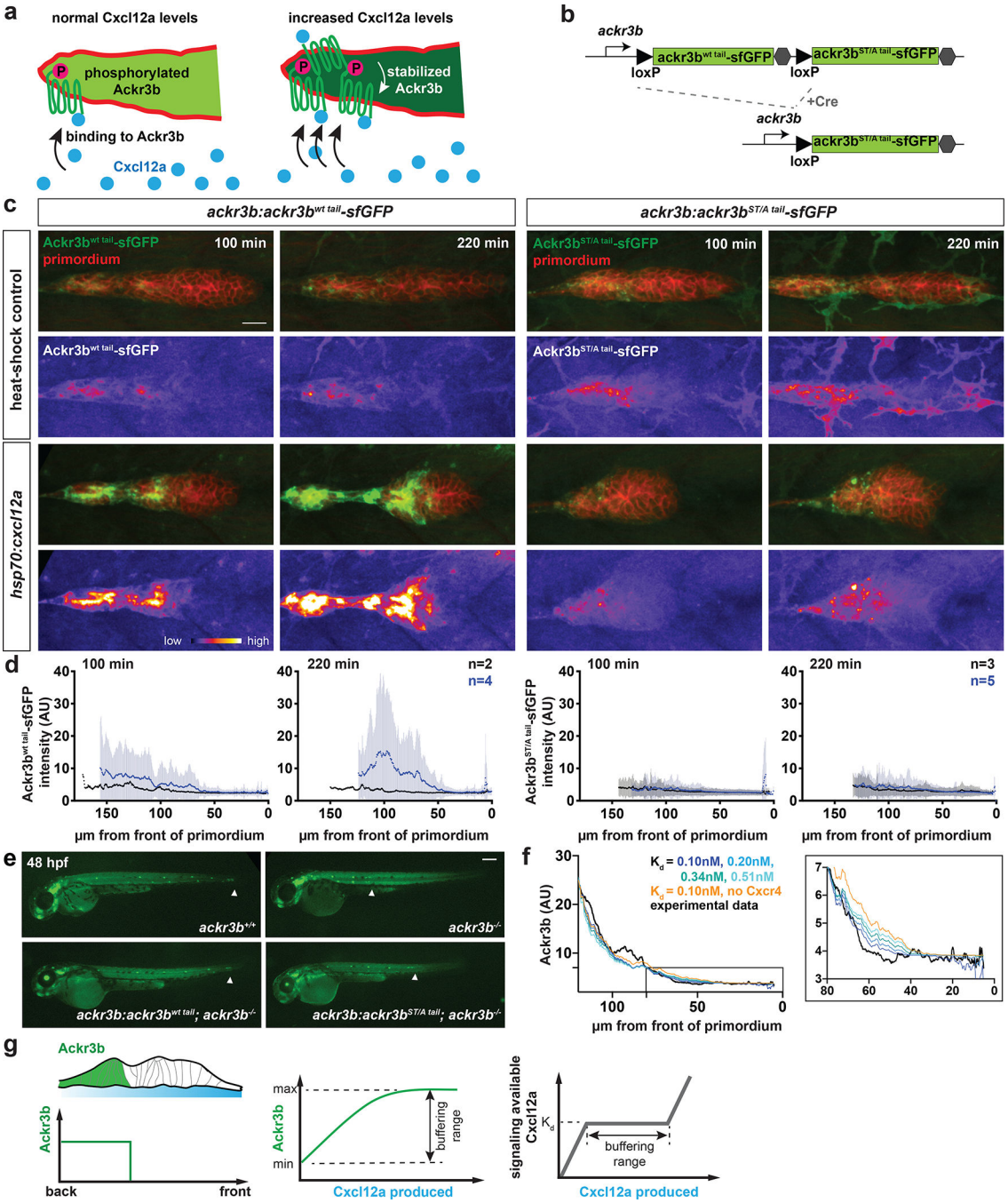

Figure 5. Ackr3b feeds back on Cxcl12a through phosphorylation to regulate primordium migration.

a. Schematic of hypothesis. Increased Cxcl12a levels lead to increased levels of phosphorylated Ackr3b which is protected from degradation and stabilized.

b. Strategy for *ackr3b-sfGFP* control and *ackr3b*$^{ST/A}$*-sfGFP* cytoplasmic tail mutant BAC transgenic lines.

c. Response of Ackr3b$^{\text{wt tail}}$-sfGFP and Ackr3b$^{\text{ST/A tail}}$-sfGFP fusion proteins in the primordium of embryos with increasing Cxcl12a levels. The control *ackr3b:loxP-ackr3b*$^{wt\ tail}$*-sfGFP-stop-loxP-ackr3b*$^{ST/A\ tail}$*-sfGFP; ackr3b−/−; prim:lyn*$_2$*mCherry* and the

experimental *ackr3b:ackr3b*$^{ST/A\ tail}$*-sfGFP; ackr3b−/−; prim:lyn*$_2$*mCherry; hsp70:cxcl12a* embryos were imaged at indicated times past a 30 min heat-shock that induced Cxcl12a expression from the heat shock promoter. The Ackr3b-sfGFP fluorescence intensities in the primordia are shown together with the primordium marker *prim:lyn*$_2$*mCherry* (top panels) and separately as a heat-map (bottom panels). The fluorescence intensities in all images are scaled identically and quantified in d. Scale bar corresponds to 20 μm. Anterior is to the left and the front of the primordium is to the right.

d. Mean Ackr3b$^{wt\ tail}$-sfGFP and Ackr3b$^{ST/A\ tail}$-sfGFP fluorescence intensities (dots) and SD (vertical bars) of heat-shocked control embryos (black, n=2 and 3 embryos, respectively) and Cxcl12a-overexpressing embryos (blue, n=4 and 5 embryos, respectively) along the front-back axis of primordia. 0 μm represents the front of the primordium.

e. Primordium (arrowhead) in *cldnB:lyn*$_2$*GFP* embryos of indicated genotypes. Note: The transgenesis marker drives sfGFP in the lens. Scale bar is 200 μm. Quantification is shown in Extended Data Fig. 5c.

f. Comparison of the modeled and measured Ackr3 concentration along the axis of the primordium for the indicated Cxcl12a-Ackr3b K_d values with and without Cxcr4b-mediated Cxcl12a internalization.

g. Summarized model. Ackr3b expression is confined to the back of the primordium where it removes Cxcl12a to generate a chemokine gradient across the primordium (left). The Cxcl12a buffering range is limited by the maximal levels to which Ackr3b can be upregulated (middle). Increasing Cxcl12a levels past this limit are not counteracted by increasing Ackr3b levels and the levels of signaling available Cxcl12a exceed the K_d of Cxcl12a for Cxcr4b (right).